ABSTRACT

Title of Thesis: CHRONOAMPEROMETRIC STUDY OF
CONFORMATIONAL RELAXATION IN PPY(DBS)

Bryan Jason West, Master of Science, 2008

Thesis directed by: Professor Elisabeth Smela
Department of Mechanical Engineering

Professor Benjamin Shapiro
Department of Aerospace Engineering

In conjugated polymer devices that switch from one oxidation level to another, such as artificial muscles, it is important to understand memory effects that stem from conformational relaxation movements of the polymer chains. Chronoamperometry during electrochemical switching of polypyrrole doped with dodecylbenzenesulfonate, PPy(DBS), is used to gain insight into the conformational relaxation kinetics. During oxidation and reduction (stepping to the anodic and cathodic voltages, respectively), an exponentially decaying current is observed, but a shoulder appears during reduction when the cathodic voltage is high enough. Subtracting an exponential curve fit from the reduction current yields a small current peak at the shoulder position. The position of this peak depends logarithmically on the applied cathodic potential, the anodic potential that was applied just prior to the reduction step, and on the time that the prior anodic voltage was held. These results are consistent with the electrochemically stimulated conformational relaxation (ESCR) model.

CHRONOAMPEROMETRIC STUDY OF

CONFORMATIONAL RELAXATION IN PPY(DBS)

by

Bryan Jason West

Advisory Committee:

Professor Elisabeth Smela (Dept. of Mechanical Engineering), Chair
Professor Benjamin Shapiro (Dept. of Aerospace Engineering)
Professor Manfred Wuttig (Dept. of Materials Science and Engineering)

Dedication

I would like to dedicate this thesis to the memory of my grandfathers: on my father's side, Bryan R. West, who taught me about the practical side of engineering through fixing everything from cars to houses, and on my mother's side, Samuel J. Caulfield, who I didn't know, but who I'm sure passed on much of his engineering inclination to me, in one form or another. I think that they would both be proud.

Acknowledgements

I would like to acknowledge the help of the following people, without whom this work, and the personal learning and growth that accompanied it, would not be possible.

My advisors: first and foremost, Dr. Elisabeth Smela, for her endless support and advice on becoming a scientist and a scholar, Dr. Benjamin Shapiro, for introducing me to the world of research, recognizing my academic potential, and providing funding to allow me to explore it through this work, Dr. Toribio F. Otero, for welcoming me to his lab and hosting my scientific and cultural experience in Spain, and Dr. Manfred Wuttig, for a calm sense of direction.

I would also like to thank all of the other people I have met at the University over the years (there are too many to list here): labmates, classmates, and friends, for giving this experience meaning by being a community for me. In particular, I thank (Dr.) Mario Urdaneta, for being not just a mentor, but a true friend during the most difficult parts of this journey.

Outside of the University, I thank those who have been close to me (family and friends who shall go unnamed here, and one who shall be named: Maria Stoica) who helped to keep life in perspective for the past three years. The degree is finished, but you are still here, and I am grateful for that.

Finally, I thank my parents, Bryan F. West and Claudia C. West, for encouraging me to pursue this degree and finish it, despite my uncertainty. It was worth it in the end.

TABLE OF CONTENTS

CHAPTER 1: INTRODUCTION

1.1 Background

In this thesis, polypyrrole doped with dodecylbenzenesulfonate, PPy(DBS), a conducting polymer, was electrochemically studied in an attempt to quantify the conformational relaxation which occurs during reduction and oxidation. Conducting polymers, and PPy(DBS) in particular, are used in actuators, such as artificial muscles, because of their ability to change volume. Previous work by the research group of Dr. Toribio F. Otero (a co-author on the journal paper in preparation as a result of this work) has extensively characterized the conformational relaxation in some types of conjugated polymers, and a model (Electrochemically Stimulated Conformational Relaxation, or ESCR) has evolved as a result. However, the model has not yet been applied to PPy(DBS). Not including conformational relaxation, PPy(DBS) has been extensively studied and characterized by many groups, including that of Dr. Elisabeth Smela, a co-advisor in this work. Therefore, the motivation for this thesis was primarily to bridge the gap between the two research groups by characterizing the conformational relaxation that occurs in PPy(DBS).

1.2 Conjugated Polymers

A conjugated polymer (CP) is a polymer containing alternating single and double bonds between repeating units. This structure allow CPs to conduct electricity when an electron is removed from one of the double bonds; the missing electron, or "hole" can move along the polymer chain. By removing electrons, CPs become positively charged (oxidized); adding electrons renders them electrically neutral (reduced). This oxidation and reduction can be accomplished

1

electrochemically, when the polymer is in direct contact with a solid conducting electrode and a liquid electrolyte.

The electrochemical switching of CPs between the oxidized and reduced states is accompanied by transport of ions in the electrolyte in order to maintain charge neutrality. I.e., upon oxidation, the net positive charge on the polymer is compensated by either cation egress or anion ingress. Upon reduction, the situation is reversed. Along with ions, water molecules, which are attached to the ions in their solvation shells, are also transported.

The ingress of ions and water molecules causes the polymer to swell, while their egress causes the polymer to shrink. This shrinking causes the polymer chains to change their conformation to a "compacted" state. Conversely, swelling is only possible if the polymer chains change their conformation to accommodate the volume taken up by the ions. This change in conformation is called "conformational relaxation" and is the focus of this study.

Since the redox can be electrochemically controlled, it follows that the swelling and shrinking can also be controlled. This controllable volume change has been used to make actuators, such as artificial muscles, using CPs as the active materials.

1.3 PPy(DBS)

The particular CP that was the subject of this research is polypyrrole (PPy), shown in Figure 1.
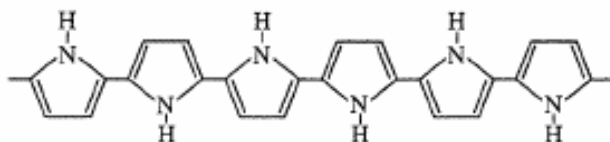

Figure 1. Chemical structure of polypyrrole (E. Smela, "Microfabrication of PPy microactuators and other conjugated polymer devices," J Micromech Microeng, 9, 1-18 (1999)).

PPy films were electrochemically polymerized while in an electrolyte solution consisting of pyrrole monomer, deionized water and the sodiumdodecylbenzenesulfonate (NaDBS; see Figure 2).
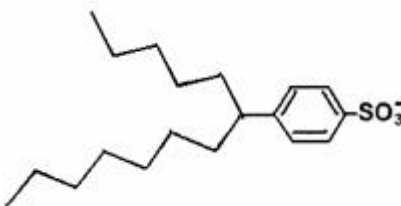

Figure 2. Chemical structure of dodecylbenzenesulfonate (E. Smela, "Microfabrication of PPy microactuators and other conjugated polymer devices," J Micromech Microeng, 9, 1-18 (1999)).

The DBS$^-$ anion is sufficiently large enough to become trapped inside the PPy chains during polymerization. Recall that during redox, ions must enter or exit the polymer to maintain charge neutrality; since the DBS$^-$ anion is immobilized, the only way for PPy(DBS) to complete oxidation and reduction is through the transport of the smaller Na$^+$ cation. Oxidation leads to Na$^+$ egress from the polymer to balance the positive charge on the PPy. This Na$^+$ egress causes the polymer to shrink (a volume decrease). Subsequent reduction of PPy(DBS) causes Na$^+$ ingress to balance the negative charge on the PPy; the Na$^+$ ingress leads to PPy swelling (a volume increase).

Because of this exclusive Na$^+$ movement, PPy(DBS) is in a sub-class of CPs that we will call "cation-transporting" materials (in contrast to "anion-transporting" materials, which are not the focus of this research). The selection of a cation-transporting material was motivated by the fact that they are easier to study and characterize; having to deal with only cation transport without worrying about anions simplifies the analysis.

1.4 Electrochemistry

In order to characterize the PPy(DBS) system, we studied it electrochemically using a potentiostat, which applies potentials while simultaneously measuring the current flowing through the system. We measured the current using two electrochemical tools: chronoamperometry (CA) and cyclic voltammetry (CV).

CA is a measure of the current vs. time and allows us to see kinetic effects. This is more useful when combined with CV, which is the study of the current vs. *voltage* in the system as it is cycled across a range of potentials, multiple times. CV was used to determine at which potentials interesting processes (e.g. ion transport) occur, since a range of potentials is applied. CA was then used, focusing on the interesting potentials and examining the kinetic effects that occur. Specifically, CA was used to study the time dependence of conformational relaxation.

CHAPTER 2: CHRONOAMPEROMETRIC STUDY OF CONFORMATIONAL RELAXATION IN PPY(DBS)

B. Jason West[a], Toribio F. Otero[d], Benjamin Shapiro[b], and Elisabeth Smela[c]*

[a]Department of Materials Science and Engineering
[b]Department of Aerospace Engineering
[c]Department of Mechanical Engineering
University of Maryland, College Park, Maryland 20742
Tel.: (301) 405-5265; Fax: (301) 314-9477; email: smela@eng.umd.edu
* author for correspondence

[d]Dpto. De Arquitectura y Tecnologías de la Edificación
Universidad Politécnica de Cartagena, ETSII
C/Carlos III, s/n, 30203 Cartagena, Spain

ABSTRACT

In conjugated polymer devices that switch from one oxidation level to another, such as artificial muscles, it is important to understand memory effects that stem from conformational relaxation movements of the polymer chains. Chronoamperometry during electrochemical switching of polypyrrole doped with dodecylbenzenesulfonate, PPy(DBS), is used to gain insight into the conformational relaxation kinetics. During oxidation, stepping abruptly to the anodic voltage results in an exponentially decaying current whose time constant decreases (i.e., the switching speed increases) with the applied voltage, but at the cost of greater consumed charge. During reduction, stepping to the cathodic voltage also results in an exponentially decaying current, but a shoulder appears when the cathodic voltage is high enough. The time constant for the exponential decay decreases even more strongly with voltage than that for the anodic current, and with the advantage that no more charge is consumed. Subtracting an exponential curve fit from the reduction current yields a small current peak at the shoulder position. The position of

this peak depends logarithmically on the applied cathodic potential, as well as on the anodic potential that was applied just prior to the reduction step. Furthermore, the shoulder position depends logarithmically on the time that the prior anodic voltage was held. These results are consistent with the electrochemically stimulated conformational relaxation (ESCR) model.

1 INTRODUCTION

The electrochemical switching of conjugated polymers between the oxidized and reduced states is employed in actuators (artificial muscles) as well as in a range of other devices, from electrochromic displays to energy storage devices (batteries, supercapacitors). This is because changing the oxidation level of the polymer is accompanied by changes in volume, color, conductivity, and other properties.

During oxidation, electrons are removed from the conjugated polymer, and during reduction they are returned. Overall charge neutrality in the material during reduction and oxidation (redox) is maintained by the ingress and egress of ions, supplied by an electrolyte with which the polymer is in contact. *Without this ion transport, the electrochemical reaction cannot proceed.* The ions are solvated, with the size of the solvation shell depending on the ion. It is thus of importance to understand how the physical processes occurring during redox control the rate of ion transport, since this determines how fast the artificial muscles can move, how fast the displays can be refreshed, or how fast the batteries can supply charge.

Conjugated polymers are polymerized in the oxidized state, with the positive charge on the polymer compensated by anions. Approximately 1 anion is incorporated into the polymer for every 3 pyrrole units. These "dopant" anions strongly affect the material properties and the switching behavior of the polymer [1,2]. For actuators, one of the most significant properties of the dopant anion is its size. As a rule of thumb, although this not always the case, if the anions are small (such as ClO_4 or PF_6), then upon reduction these anions exit the polymer, and during oxidation small anions from the electrolyte re-enter [3,4]. However, if the anions are sufficiently large (such as dodecylbenzenesulfonate (DBS) or polystyrenesulfonate (PSS)), then they can be trapped in the polymer, particularly in polymers such as polypyrrole (PPy) that are crosslinked. Since the anions cannot exit the material upon reduction, charge neutrality is primarily maintained by the ingress of cations, which subsequently exit the material again during oxidation. The ingress of ions leads to a volume expansion, and their egress to contraction, which is exploited in actuators. The various redox states are illustrated schematically in Figure 3.
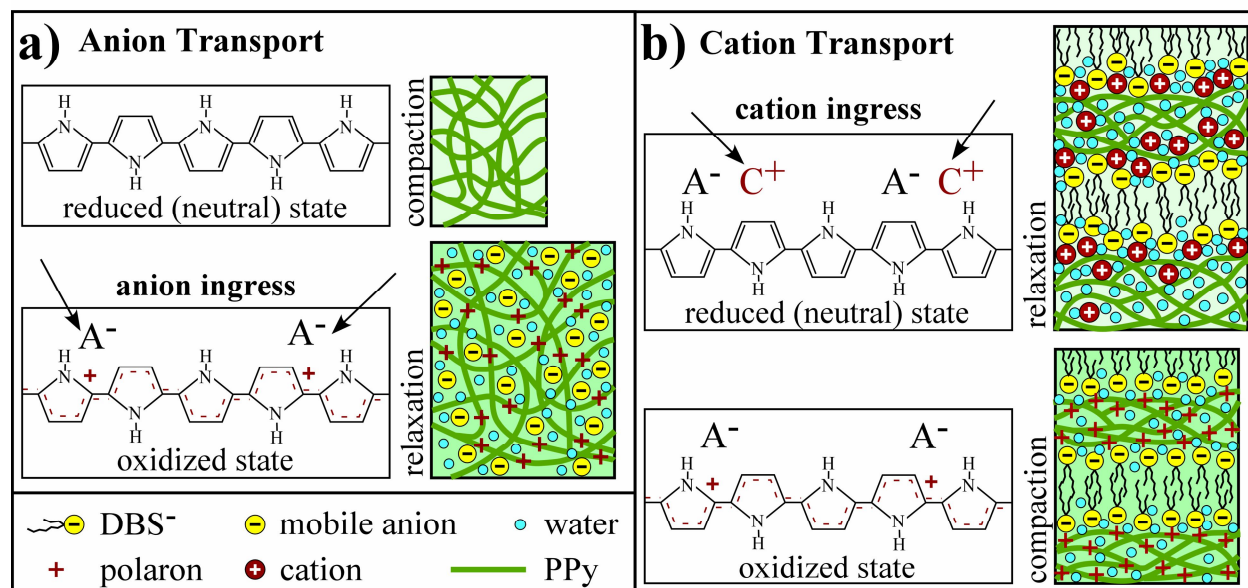
Figure 3. **Schematic illustration of redox in a) a general anion-transporting PPy and b) the cation transporter PPy(DBS), which has a lamellar structure. In a), hydrated anions enter the polymer during switching to the oxidized state to maintain charge neutrality, which requires PPy chain relaxation. In b), hydrated cations enter during switching to the reduced state, which also requires relaxation.**

The ingress of ions requires the creation of free volume in the material, which takes energy. This is a key concept. This electrical energy supplied during electrochemical switching is consumed by the electrochemical reaction itself, by the movement of the ions, and by conformational movements of the chains.

If the polymer is initially in a compact state that the ions cannot enter, then additional energy is required to allow the chains to change conformation and move apart[***]: the rate limiting step of

---

[***] The matrix can be considered closed when the average distance between neighboring polymeric chain segments is smaller than the size of the solvated ion [5].

the reaction (oxidation or reduction rate) becomes the conformational relaxation rate. The

dependence of the ion ingress on the degree of compaction of the polymer has been thoroughly

studied in anion-transporting materials and has been well described using the electrochemically

stimulated conformational relaxation (ESCR) model [6-8]. The ESCR model has been shown to

account for behavior in a wide range of materials under a wide range of experimental conditions.

In chronoamperograms of anion-transporting polymers, conformational relaxation manifests

itself as a peak in the anodic (oxidation) current (please see Figure 25 in the Discussion section

for an example) whose position in time depends on experimental parameters such as the applied

anodic voltage [6-8], the cathodic voltage applied preceding the anodic step [6-11], the time

spent at that cathodic voltage [12-14], the temperature [6-8,15,16], the solvent [17], the size of

the ion [5], the type of polymer [7], the number of cycles performed [18], and the electrolyte

concentration [8]. There is no corresponding cathodic (reduction) peak during anion egress,

since the polymer is in the expanded state and already has the necessary free volume to allow ion

movement [19].

This coupling of ion ingress, volume change, and energy is the basis of the use of conjugated

polymers as artificial muscles. (On the other hand, it is problematic for electrochromic and

energy storage applications that do not require the volume change, but that must take it into

account: if the polymer could be kept in the expanded state, then these devices could be

switched faster.) It is also important to understand conformational relaxation effects since they

give the polymer a "memory": the previous state (oxidized or reduced) of the polymer, and how

long it was held there, can affect how quickly it responds to a stimulus to change its oxidation

level. The conformational energy is not only the origin of the actuation of conjugated polymers, but also of their sensing properties. The link between conformational energy and electrochemical energy allows these materials to be used as load sensors (and thus to be used in feedback-control systems) [20,21], chemical sensors [22], and thermal sensors [22], since mechanical force, chemical reactions, and temperature all affect the conformational energy, which can be measured electrochemically. Mathematical models that quantify how the conformational relaxation and memory affect the redox speed must therefore be included in control schemes for conjugated polymer devices.

To understand the complex interrelationships between ion movements, chain conformations, and energy (and eventually develop mathematical models), it is necessary to control the experimental conditions so that the reaction is controlled by a single rate-limiting step. In this paper, we are concerned with the conformational changes in the polymer, so the experiments were designed to establish a particular state of the polymer matrix prior to electrochemical switching, and to keep the other variables constant.

Cation-transporting materials are important in actuators [23-26], but conformational relaxation in these materials is not yet understood. In this work we examine conformational relaxation effects in PPy doped with DBS, PPy(DBS), which has been used extensively, particularly in microactuators [23,24]. We examine the chronoamperograms of PPy(DBS) as a function of oxidation and reduction potentials, as well as the time held at an oxidizing potential. It is known that higher cathodic (negative) potentials increase the speed of the reduction reaction by increasing the speed of cation migration [27] (recall that ion ingress occurs during reduction).

Based on ESCR, it is expected that higher cathodic potentials will also lead to faster responses by providing greater energy for chain movements. (Energy and voltage are directly related; see equation (2).) Higher anodic potentials, on the other hand, are expected to increase the degree of compaction of the polymer matrix, slowing down subsequent reduction reactions by bringing them under increasing conformational relaxation control; this is what is meant by the memory effect that was discussed earlier. The degree of polymer compaction has already been observed to affect cation mobility in PPy(DBS), with mobility increasing strongly as the polymer takes on an increasingly open state during the reduction process [28].

The behavior of PPy(DBS) is expected to differ from that of anion-transporting PPys not only because cations enter during reduction, rather than anions entering during oxidation, but because the DBS that is incorporated during material synthesis is a surfactant that imparts a lamellar morphology to the PPy [29] (Figure 3), which none of the examined anion-transporting polymers have had. Ion transport parallel to the lamellae is faster than perpendicular to them, through the PPy chains, and out-of-plane expansion is much greater than inplane expansion. (This concept is not the focus of this study, but will be discussed throughout the paper to aid in interpretation of the results.) Although we do not specifically study this structure, it would be expected to strongly influence phenomena such as nucleation [6], which plays a strong role in producing the peak in the chronoamperogram of the anion-transporters. Nucleation has not been observed in PPy(DBS); instead, a uniform cation-ingress front is seen [30].

Only one predominantly cation-transporting system has been studied previously: PPy(p-toluenesulfonate), or PPy(pTS), cycled in propylene carbonate containing $LiClO_4$ [19]. Unlike

11

in anion-transporting polymers, ESCR manifested itself as a small shoulder on a decaying cathodic current. The anodic current decayed smoothly (see Figure 25 for an example plot).

According to the ESCR model, relaxation (chain opening) is governed by an Arrhenius law [19]:

(1) $\qquad \tau_r = \tau_0 e^{\Delta H / RT}$

where τ_r is the time it takes for the relaxation, τ_0 is a time constant, and ΔH is the molar enthalpy. This energetic term depends on the applied potentials through

(2) $\qquad \Delta H = \Delta H^* + \Delta H_c - \Delta H_r$

$\qquad \Delta H \sim z_c \eta_c - z_r \eta_r$,

where the first term ΔH^* is the molar conformational energy consumed in the absence of electric fields, and has been determined to be on the order of 10-30 kJ/mol in various polymers [7]. The second term ΔH_c is the increment of conformational energy due to the closure of the polymer matrix. It is proportional to the compaction overpotential $\eta_c = E_c - E_s$, in which E_c is the applied compaction (in this case, anodic) potential and E_s is the closure potential, defined as the voltage at which the matrix begins to close. (When comparing with prior work, it is important to keep in mind that for predominantly cation-exchanging materials, such as PPy(DBS), the compaction overpotential is an anodic, rather than a cathodic, overpotential.) In other words, the higher the compaction overpotential that is applied prior to the reduction step, the higher the molar enthalpy, and thus the longer the relaxation time τ_r during reduction. The third term ΔH_r is the electrochemical energy that contributes to matrix relaxation, proportional to $\eta_r = |E_r - E_0|$, where η_r is the relaxation (in this case cathodic) overpotential, E_r is the reduction potential, and E_0 is

the potential at which reduction begins (and the structure starts to open). So, the higher the potential that is applied during reduction, the lower the molar enthalpy, and the faster the conformational relaxation will take place. The constants z_c and z_r correspond to the charge required to compact or relax one mole of polymer segments, respectively.

According to the ESCR model, the time spent holding the polymer at the compaction potential, denoted as t_{wait}, also affects the molar enthalpy through z_c [12]:

$$(3) \qquad z_c = z_c^0 + \frac{RT\alpha}{\eta_c} ln \, t_{wait},$$

where z_c^0 includes only potential-related contributions. The longer the time t_{wait} that the polymer is allowed to compact (at the anodic potential for PPy(DBS)), the greater amount of energy that is required to relax the polymer segments, and the higher the molar enthalpy.

In PPy(pTS), the position of the shoulder, in time, as a function of the reduction potential was estimated by taking the second derivative of the chronoamperogram. This time, t_{ESCR}, had the expected logarithmic dependence,

$$(4) \qquad \ln(t_{ESCR}) = C' - z_r \eta_r / RT$$

consistent with the ESCR model. The constant z_r was calculated to be 2400 C/mol, comparable to values found for anion-transporting materials [7]. The occurrence of shoulders rather than peaks is probably due to the fact that the material always contains charges ($[PPy^{n+}(pTS^-)_n]$ in the oxidized state and $[PPy(pTS^- \bullet Li^+)_n]$ in the reduced state), resulting in a significant water content at all times (since dipolar water molecules interact strongly with charged species). This would make it difficult for the polymer to reach a state of deep compaction.

In this work, we show that the behavior of PPy(DBS) is similar to that of PPy(pTS), with smooth current decays upon oxidation and small shoulders upon reduction. The shoulder occurs sooner when the reduction (relaxation) potential E_{ca} is increased. By deconvoluting the current into an exponential decay component and an ESCR peak component, the peak time is found to decrease logarithmically with E_{ca}, as expected by the ESCR model. The peak position increases logarithmically with the oxidation (compaction) potential E_{an}, and it increases with the time that E_{an} is held, also consistent with the ESCR model.

Table I. Variables used in the paper.

Variable	Meaning
τ_r	time it takes for the relaxation
τ_0	time constant for relaxation
ΔH	molar enthalpy of relaxation
ΔH^*	molar conformational energy consumed in the absence of electric fields
ΔH_c	increment of conformational energy due to the closure of the polymer matrix
ΔH_r	electrochemical energy that contributes to matrix relaxation
η_c	compaction overpotential (anodic for PPy(DBS))
η_r	relaxation overpotential (cathodic for PPy(DBS))
$E_c = E_{an}$	applied compaction (= anodic) potential
E_s	closure potential: voltage at which the matrix begins to close
$E_r = E_{ca}$	applied relaxation (= cathodic) potential
E_0	opening potential: voltage at which reduction begins and the structure starts to open
z_c	charge required to compact one mole of polymer segments
z_r	charge required to relax one mole of polymer segments
t	time
t_{ESCR}	position of the ESCR peak in time
I	current
I_0	current at $t = 0.2$ s
τ	relaxation time of the exponential current decay
β	stretching coefficient
ε	RMS error of the exponential fit to the current decay
Γ_1, Γ_2	regions of the chronoamperometric curve fit by the exponential
$t_{0.5}$	time at which the exponential current has decayed to half its initial value
R	ideal gas constant
T	temperature
Q_{an}	charge consumed during the anodic step
Q_{exp}	charge under the fitted exponential
Q_{ESCR}	charge in the subtracted (ESCR) peak
v	ion migration velocity

2 METHODS

2.1 Experimental

2.1.1 Substrate Preparation

The substrates on which the PPy was deposited were sections of oxidized, 500 μm-thick Si wafers coated with 30 Å of Cr and 2000 Å of Au by thermal evaporation (Cooke, 80 A, $5x10^{-6}$ Torr, 5 Å/sec). These surfaces were flat and mirror-smooth, as seen visually and by atomic force microscopy and profilometry [31,32].

Because of the perfect smoothness of the surfaces [31] on clean Au the PPy delaminated during cycling, preventing the completion of the desired series of experiments. It is known that delamination of PPy(DBS) films from smooth Au can occur after a relatively small number of cycles [32]. Thus, just prior to PPy deposition, the wafer sections were immersed into a 1 mM (5 vol%) solution of α-lipoic acid (Aldrich) in ethanol for 24 hours. Treatment with α-lipoic acid was based on the supposition that the two thiol moieties of this molecule would stabilize the monolayer during electrochemical cycling [33]. (Monolayers with a single thiol are completely removed during electrochemical cycling [34,35]. No delamination occurred on the treated surfaces, based on unchanging total charge and unvarying peak positions during cyclic voltammograms taken throughout the course of the experiments. (This does not, however, establish the efficacy of the treatment, since untreated samples have a wide range of lifetimes [36]. Further tests are required to show that the α-lipoic acid definitely improves adhesion.)

2.1.2 Polymerization

The pyrrole monomer was sieved through AlO_2 powder (Aldrich) before use. Polymerization

was performed potentiostatically in a solution of 0.1 M pyrrole (Sigma-Aldrich) and 0.1 M

NaDBS (Aldrich) in de-ionized water. The Au on the wafer section served as the working

electrode (WE). It was immersed to a depth of 2.0 cm into the solution and held in place with a

toothless Cu alligator clip (not immersed; positioned above the solution). An Autolab

EcoChemie potentiostat (pgstat30) was used to apply a constant 0.46 V vs. an Ag/AgCl reference

electrode (BAS, Inc.). The counter electrode (CE) was a 5 cm x 2 cm x 0.5 cm porous carbon

plate. The working electrode was secured approximately 4 cm from the counter electrode so that

their surfaces were facing each other and parallel. The reference electrode was 1 cm from the

working electrode. Film thickness was controlled by ending the polymerization after 100

mC/cm^2 of charge had been consumed, which resulted in 5000 Å-thick PPy films, determined by

film color [37]. The low voltage leads to films of uniform thickness. The average current

density during polymerization was 64 $\mu A/cm^2$ and remained relatively constant throughout

polymerization. The mass of the films was estimated to be 19 μg, using the dimensions of the

film and values of PPy density reported in the literature [38,39][*]. After PPy deposition, the

wafer sections were scribed into pieces 0.5 cm wide and 3.0 cm long.

---

[*] The effective film volume V was calculated using length = depth immersed into electrolyte = 0.5 cm, width = sample width = 0.5 cm, and thickness = 5000 Å = $5*10^{-5}$ cm, giving V = $1.25*10^{-5}$ cm^3. Using a density of 1.5 g/cm^3, film mass = $1.25*10^{-5}$ cm^3 * 1.5 g/cm^3 = $1.88*10^{-5}$ g.

2.1.3 Cycling

Electrochemical cycling was done by immersing the films to a depth of 0.5 cm (for square-shaped immersed areas of 0.25 cm^2) into a 0.1 M aqueous solution of NaDBS, with the electrochemical cell arranged the same way as during polymerization. Switching in NaDBS ensured that only cation transport took place. (In electrolytes such as NaCl, Cl$^-$ transport occurs in parallel [40], which complicates data analysis.) The cell was covered with Parafilm M (Pechiney) to prevent evaporation during the long course of the experiments (approximately 10 hours). Solution pH was monitored during cycling with universal indicator strips (EMD colorpHast); the solution was replaced if the pH drifted more than one unit from neutral.

Cyclic voltammetric (CV) scans were performed between -1.0 V and +0.4 V at 25 mV/s vs. Ag/AgCl. Chronoamperometric scans (CAs) were performed using a programmed potential stepping routine, which applied alternating anodic and cathodic potential steps, each of 5 seconds duration (Figure 4). Anodic potentials were first varied in a series, incrementally from -0.2 V to +0.4 V, by 0.05 V. Note that all of these potentials were above the oxidation peak. A constant cathodic potential step was applied between each anodic step. The anodic potential series was repeated for incrementally-increasing cathodic potentials in steps of 0.05 V from -0.7 V (within the region of the reduction peak) to -1.4 V (at which hydrolysis occurs). Two CV scans were performed before each CA series, both to ascertain the state of the PPy film and to "erase" any memory effects that may have been induced by the sequence. The entire process was completed separately on three samples, varying the cathodic potentials in the opposite direction (from -1.4 V to -0.7 V) on one sample (sample 2). The order did not affect the results. In the results,

representative data from only one sample are presented; to see results from all three samples, please refer to the supporting information.
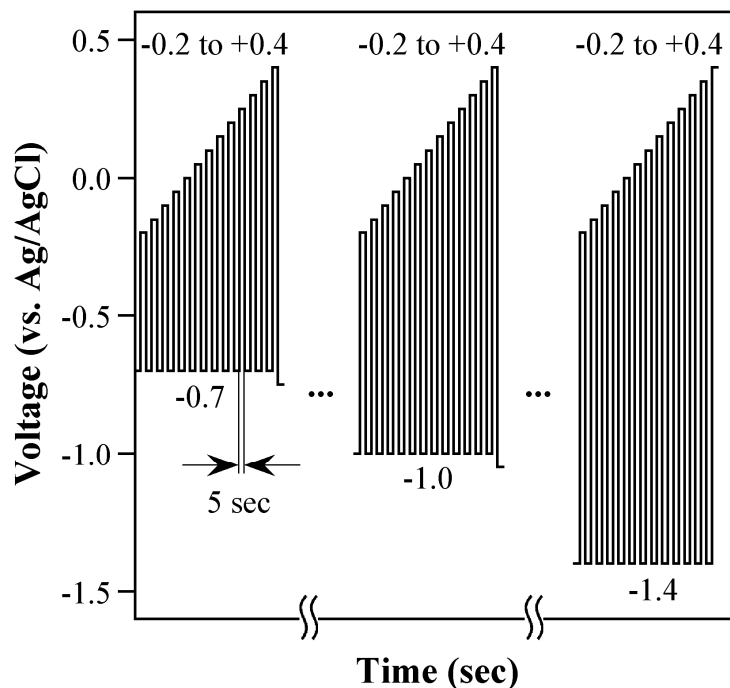

Figure 4. Illustration of the series of potentials that were applied during chronoamperometry. Voltages were stepped from a given cathodic potential, held for 5 sec, to a series of anodic potentials between -0.2 and +0.4 V in increments of 0.05 V, also held for 5 sec. Two cyclic voltammograms were then performed between +0.4 and -1.0 V, the cathodic potential was lowered by 0.05 V from the previous series of steps, and the series repeated. Stepping to only 3 cathodic potentials is illustrated, with the remaining ones and the CVs represented by ellipses, "...".

In holding time experiments, the potential was switched between a fixed cathodic potential, -1.0 V held for 5 seconds, and a fixed anodic potential, 0.0 V, held for increasingly longer times: 1, 2, 5, 10, 20, 50, 100, 200, 500, and 1000 seconds. These experiments were also repeated on 3 samples.

During electrochemical switching, no evidence of nucleation was observed.[*] The Au surfaces were smooth down to the nm level, giving the PPy great homogeneity, with no preferred nucleation sites. There was, however, visual confirmation of fast lateral ion transport from the edges of the sample toward the center. This occurred simultaneously with a color change at the center of the film due to vertical ion transport from the electrolyte/film interface toward the electrode. This is well-known in PPy(DBS) and is due, as mentioned above, to its lamellar microstructure [29,41].

2.2 Data Analysis

2.2.1 Anodic Chronoamperograms

To quantify the speed of the oxidation reaction, stretched exponential curves were fit to the anodic chronoamperograms (Figure 5). (This choice is discussed in the Supporting Information.) The stretched exponential function is given by [42,43]

$$(5) \qquad I = I_0 e^{(-t/\tau)^{\beta}} , \ 0 < \beta \leq 1$$

where I is the current, I_0 is the initial current, τ is a relaxation time (not the same as τ_r in equation (1)) , t is the elapsed time, and β is the stretching coefficient. Stretched exponentials have been used to fit a range of relaxation behaviors, with β being an empirical value [44]. Of relevance to its use here with PPy redox, such a function can be used to describe a system with a distribution of relaxation times, for example due to different local environments or conjugation lengths.

---

[*] Because PPy is electrochromic, the switching reaction can be monitored visually as a color change. Nuclei thus appear as small spots of a different color that grow outward and coalesce.

Stretched exponentials have previously been fit to the CAs of conjugated polymers when the redox process is not under conformational relaxation control (i.e., to the cathodic current decays in anion-transporting materials) [7]. It should be noted that such a fit corresponds to the ESCR model in the absence of conformational relaxation [6]:

$$(6) \qquad I_d(t) \; = \; bQ_d e^{-bt} \; ,$$

where b is a constant related to the diffusion coefficient inside the swollen film and Q_d is the charge due to ion diffusion.

In the stretched exponential function in equation (5), I_0 was set equal to the initial current, which was the current at $t = 0.20$ sec. Values prior to this were discarded in both the anodic and cathodic steps because during this time, there was capacitive charging of the Au (see Figure 7). The values for τ and β were determined through an iterative process using a Matlab script. The best fitting combination was deemed to be the one that resulted in the smallest RMS error ε, where ε is the sum of the differences between the data points of the experimental curve and the fit between $t = 0$ and 5 sec. The data could be well fit ($\varepsilon < 0.01$) using just two values of β: $\beta = 0.95$ for anodic voltages -0.15 V $< E_{an} < 0$ V, and $\beta = 0.85$ for $E_{an} > 0$ V. (The two values might arise from moving from the electrochemical reaction in Gauss 2 to the pseudo-capacitive process which occurs above that; see Figure 6. These two reactions may have different time constants.)
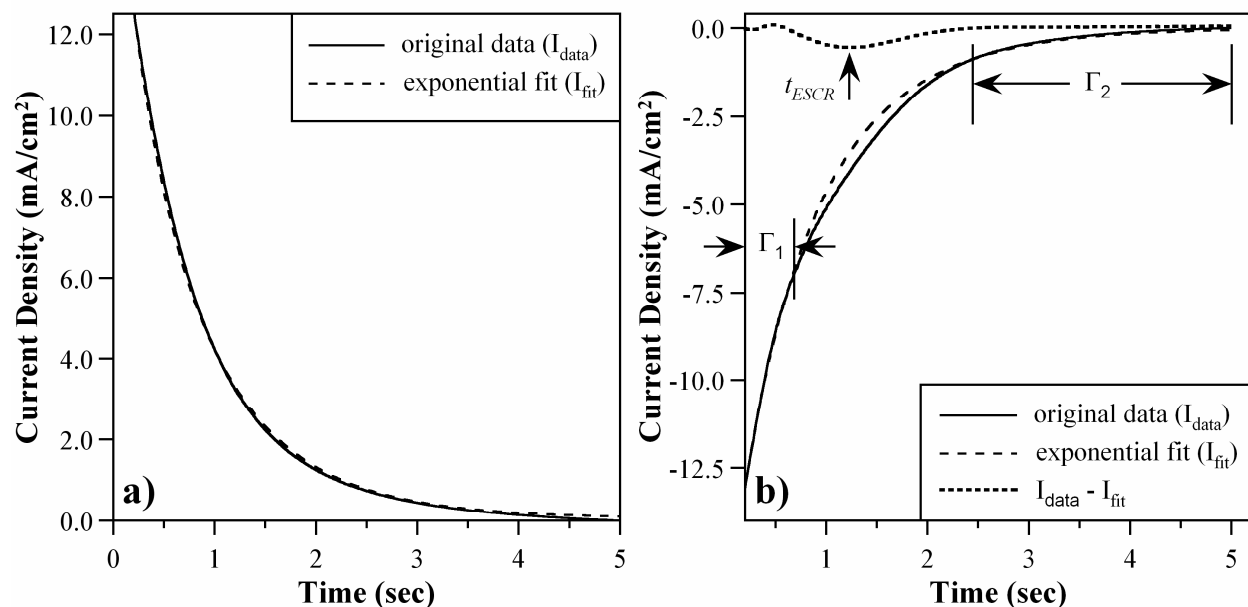
Figure 5. **a) Stretched exponential curve fit (dashed line) to an anodic CA (solid line), in this case a step from -1.40 to +0.10 V; $\beta = 0.85$. b) Exponential curve fit to the beginning and end of a cathodic CA, in this case a step from +0.40 to -1.00 V. The difference between these curves (dotted line) is also indicated; this is termed the ESCR peak, and the time at which the peak occurs is t_{ESCR}.**

2.2.2   Cathodic Chronoamperograms

The shoulders in the cathodic chronoamperograms of PPy(DBS) were even smaller than those for PPy(pTS) [19]. Thus, the method of locating the peak position by taking the second derivative of the curve could not be used. To examine the nature of the current component that gave rise to the shoulders in the cathodic CAs, these curves were therefore also fit with exponentials,

(7) $\qquad I = I_0 e^{-t/\tau}$,

but these were not stretched (i.e., they had $\beta = 1$). (There were not always sufficient data on either side of the shoulder to allow an accurate determination of β, and using $\beta = 1$ gave good results, with $\varepsilon < 0.01$.) To ensure that the fit matched the initial current density, the curve was constrained to intersect with the first considered experimental data point at $t = 0.20$ seconds. At potentials more cathodic than -1.0 V, at which the shoulder was clearly evident, the exponential was fit only to the sections of the curve before and after the shoulder (denoted Γ_1 and Γ_2, respectively, in Figure 5b). As the shoulder grew or moved to shorter times, Γ_1 shrank to zero.

Fitting of τ was done by starting with large Γ_1 and Γ_2 (in the extreme case, covering the entire CA) and incrementally decreasing their size until the RMS error of the fit in both of those regions reached a steady minimum value. Too large a Γ_1 required the exponential to pass through the shoulder, thus making it decay too slowly and introducing a large RMS error in the region of Γ_2. Likewise, too large a Γ_2 also required the exponential to pass through the shoulder, again making it decay too slowly and introducing a large RMS error in the region of Γ_1. Incrementally reducing Γ_1 and Γ_2 until the error no longer decreased forced the exponential to fit only the portions of the CA away from the shoulder, while at the same time keeping Γ_1 and Γ_2 as large as possible to ensure the most accurate fit to the exponential. The fitted exponential was then subtracted from the original data, revealing what we shall refer to as the ESCR peak (dotted line in Figure 5b).

3   RESULTS

3.1   Cyclic Voltammetry

The endpoint potentials used during the chronoamperometric studies were chosen based on cyclic voltammograms. The CVs also provided a means of monitoring film electroactivity and adhesion, and provided insight for understanding the CA results.

Typical CVs for PPy(DBS) and a clean Au surface are shown in Figure 6a. The oxidation and reduction peaks of the PPy occur at approximately -0.40 V and -0.45 V vs. Ag/AgCl, respectively. Shoulders are visible for both processes at -0.55 V and -0.65 V. The processes associated with the oxidation peak are essentially complete at -0.2 V, indicated by a leveling-off of the current. (The origin of the constant, so-called "capacitive" current above this peak, seen here between -0.2 V and +0.4 V, has been attributed to a variety of causes, and is still the subject of controversy. The magnitude of this charge in PPy(DBS) has been shown to be highly dependent on the polymerization conditions, being entirely absent in some cases [45].) The reduction processes are complete by -0.90 V, and the large cathodic current beyond -1 V is due to hydrolysis. The ranges of endpoint potentials used in the CA experiments are indicated by the hollow arrows. Note that the anodic endpoint potentials are all above both oxidation peaks, and the cathodic potentials are all below the first reduction peak.
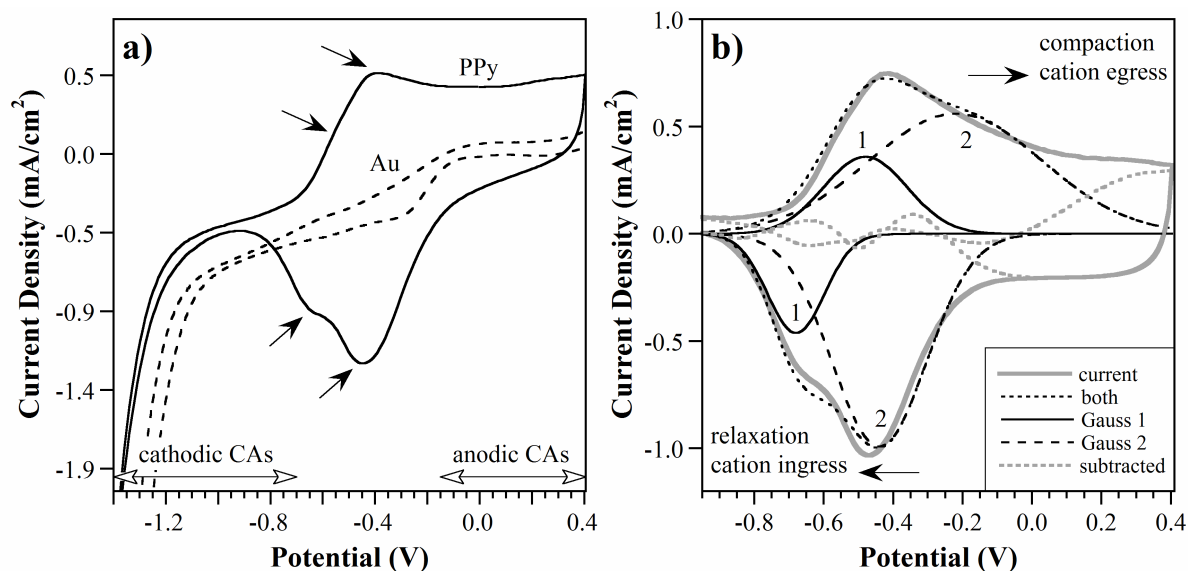
Figure 6. **a) Equilibrated cyclic voltammogram taken at 25 mV/s of a 5000 Å thick PPy(DBS) film and of an uncovered Au film. Solid arrows point to the two pairs of oxidation and reduction peaks. b) The PPy CV after it was corrected for IR drops, and dual Gaussian curve fits to the peaks. The charge densities under Gaussian peaks 1 and 2 are 1.08 mC/cm^2 and 3.46 mC/cm^2, respectively.**

The CVs from the three samples that were tested all showed identical peak positions after 10 break-in cycles. It should also be noted that there was no noticeable cathodic shift of the reduction peaks due to compaction upon cycling to +0.4 V, compared to the peak positions when cycling to an upper voltage limit of only -0.2 V.

The two pairs of peaks in the CV can be approximated by two pairs of Gaussians that have been constrained so that the charge in each Gaussian of the pair is equal [28] Such a dual Gaussian curve fitting is shown in Figure 6b after the CV was corrected to remove IR drops [31].

Previously, both color and volume change in PPy(DBS) have been found to be associated only with the smaller, more negative pair of peaks, "Gaussian 1" [28], which consume only ~20% of

25

the total charge. The primary charge-consuming process represented by "Gaussian 2" is still not clear. The so-called capacitive charge is the charge that remains after subtracting the two Gaussians from the original CV.

During chronoamperometry, the currents from all the electrochemical processes that are capable of occurring at that potential flow simultaneously. It is therefore more difficult to characterize each component of the total CA current separately.

3.2   Chronoamperometry: Overview

A typical CA is shown in Figure 7. The anodic step (positive current) causes the oxidation reaction to occur, with corresponding cation egress, while the cathodic step (negative current) reduces the film and leads to cation ingress. The current levels off by or before 5 seconds, indicating the completion of the switching process.
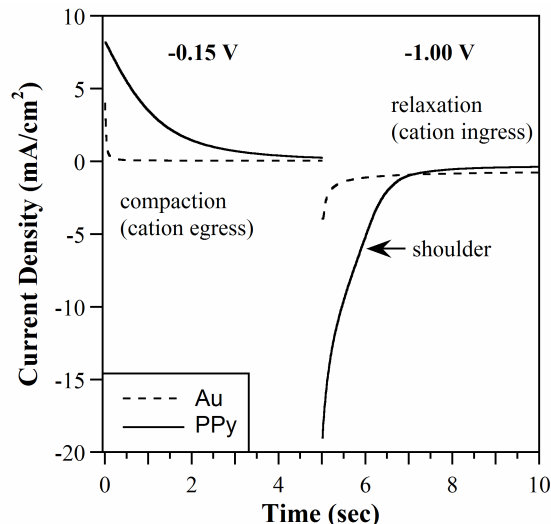
Figure 7. Typical chronoamperograms, before subtraction of baseline currents, for PPy(DBS) and for Au upon stepping from -1.00 V to -0.15 V and back again. Each potential was held for 5 seconds.

The CA data were processed by subtracting the baseline current (~0.1 mA) that continued to flow after the reduction process was complete. During reduction, the baseline current is due to hydrolysis (see Figure 6a), since the PPy-related processes have been completed after 5 seconds. These currents also occurred on bare gold working electrodes, after the capacitive charging during the first 0.2 seconds had stopped. (As mentioned above, because of that charging, the first 0.2 seconds of CA data from the PPy samples were disregarded during data analysis.)

Just as seen in PPy(pTS) [19], there was a shoulder on the cathodic curve, although in PPy(DBS) the shoulder was smaller. In the following sections, we examine the voltage-dependent behavior of the CAs, beginning with the anodic step before going on to the more complex cathodic step.

3.3 Chronoamperometry: Anodic Currents

In this section, the oxidation reaction is investigated, in which the polymer transitions from a state of low electrical conductivity to one of high conductivity and from an expanded state filled with cations to a more compacted state. The roles of the initial cathodic potential and the final anodic potential on the anodic currents are studied. Since the polymer matrix begins in an open state in all cases, no conformational relaxation effects are expected. The rate of ion transport is expected to be influenced solely by the magnitude of the electric fields (since all of the other electrochemical variables, e.g. temperature and electrolyte concentration, were held constant).

3.3.1 Overview of Results

Both the anodic potential applied during the step and the cathodic potential that had been applied before the step were examined for an impact on the current decay. Figure 8a shows CA curves resulting from steps to different anodic potentials E_{an} from a fixed initial cathodic potential E_{ca} of -1.4 V[*], and Figure 8c shows CAs from different cathodic potentials E_{ca} to a fixed anodic potential E_{an} of +0.4 V[**]. Note that "increasing E_{ca}" in this figure, and in all subsequent figures, means increasingly large cathodic voltages, i.e., going in the direction from -0.70 to -1.40 V.

---

[*] Recall that initial cathodic potentials E_{ca} were examined throughout the range from -0.7 to -1.4 V, but just the one series is shown here.

[**] Again, only one series is shown, although data were collected for E_{an} from -0.15 to +0.40 V.
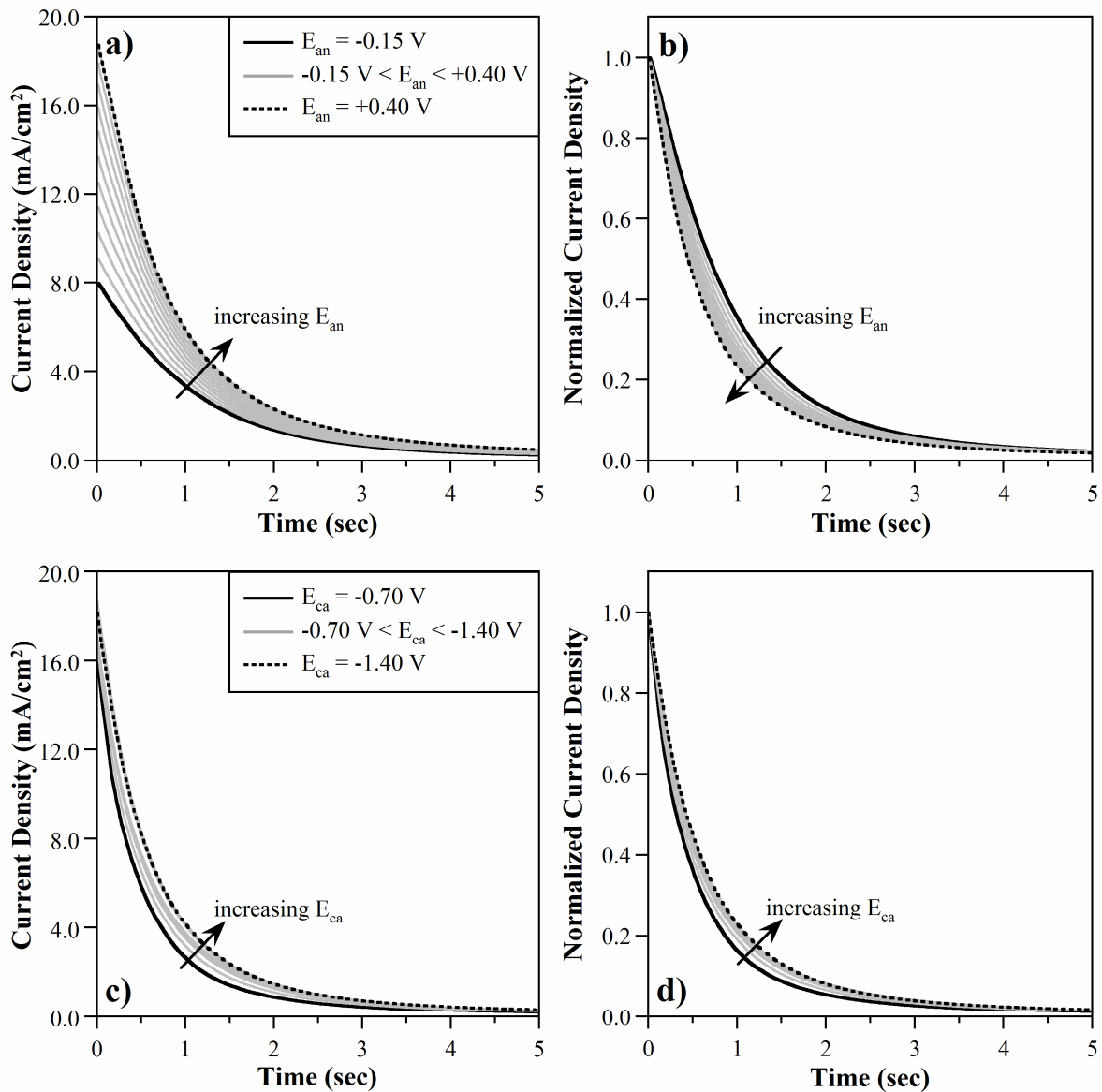
Figure 8. **a) Anodic currents upon stepping to different anodic potentials from a fixed cathodic potential (-1.40 V). b) The same data normalized by the initial current density. c) Anodic currents upon stepping to a fixed anodic potential (+0.40 V) from different initial cathodic potentials. d) Normalized versions of the curves in c).**

Looking at the current density in Figure 8a, the initial current I_0 increased with E_{an}, from 8.0 to 18.0 mA/cm^2, consistent with the CVs, which showed continued charge consumption with

increasing E_{an} even above the oxidation peak. Despite these differences in I_0, however, all the currents had decayed to constant values (comparable to the hydrolysis current, discussed in section 3.2) by $t = 5$ seconds.

The time dependence of the reaction only becomes apparent when the curves are normalized, as in Figure 8b. The oxidation speed increased with increasing anodic voltage, as expected theoretically for the oxidation of a thin film of PPy(DBS) [46]. Taking the time at which the current had decayed to half its initial value, $t_{0.5}$, as a rough measure of the speed, one can see that for $E_{an} = -0.15$ V, $t_{0.5} = 0.7$ seconds, while for $E_{an} = +0.4$ V, $t_{0.5} = 0.45$ seconds (Figure 9a). One can also examine the time it takes the current to fall to 10% of its initial value, $t_{0.9}$, which better reflects the behavior in the "tails" of the peaks. The time fell by a larger amount in going from $E_{an} = -0.15$ V to $E_{an} = +0.4$ V, from 2.3 to 1.8 seconds, for a difference of 0.5 sec.
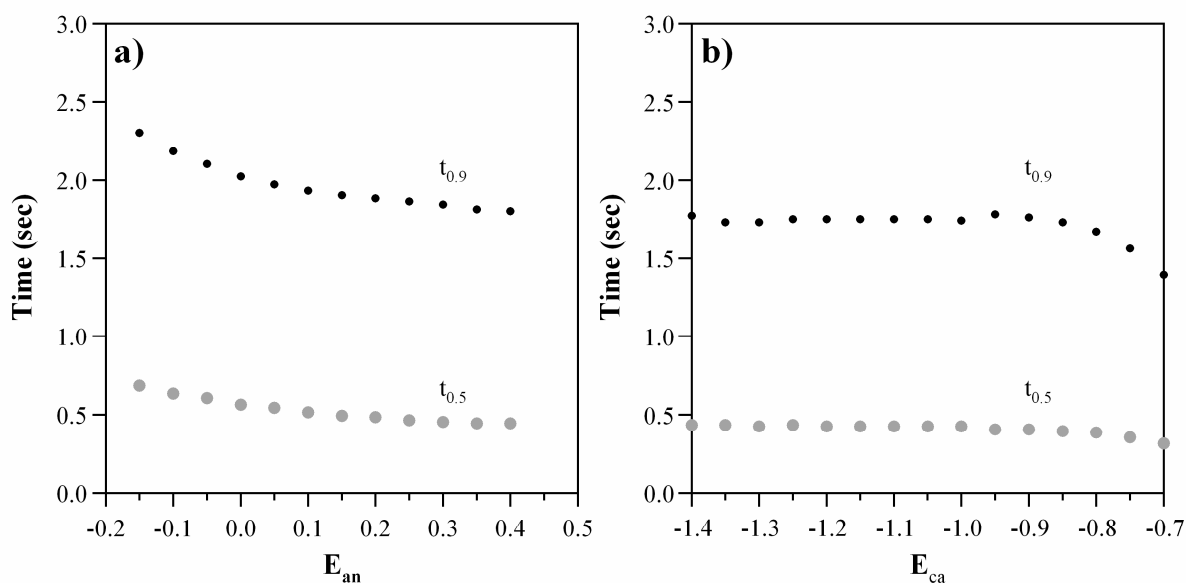
Figure 9. Time required for the anodic currents in Figure 8 to fall by 50% and 90% as a function of a) E_{an} and b) E_{ca}.

For actuators, these results suggest that it may be possible to speed up the movement during oxidation, by about half a second at these film thicknesses, by raising the anodic voltage from -0.15 to +0.4 V, but at the cost of a hefty 90% increase in consumed charge, from 2.35 to 4.5 mC/cm^2 (obtained by integrating the areas under the CAs; plots of the charge are included in the Supporting Information). Since the *extent* of movement is not increased by raising the voltage in this anodic range [28,47][*] (in which the polymer is fully oxidized), this speed would come at a cost of a lower efficiency, defined as mechanical work output divided by energy input, since the same movement is achieved but requires greater current. This discussion assumes,

---

[*] Within the potential range of the peaks in Gaussian 1, the movement is a linear function of the charge consumed during Gaussian 1 in PPy (DBS) (see for example Figure 18 in [28]). However, in these CAs the potential limits are beyond that (as shown in Figure 6a), and lie in the region where charge is consumed with no associated movement.

however, that the volume change (associated with Gaussian 1) happens with the same time dependence as the total current shown in Figure 8, but this is not necessarily the case. Additional work, outside the scope of this paper, would be required to confirm this.

Figure 8c shows the effect of stepping to a fixed E_{an} = +0.40 V from a series of increasingly cathodic initial potentials E_{ca} between -0.70 and -1.40 V. The anodic current increased somewhat as E_{ca} was raised from -0.70 to -1.00 V, and thereby moved over the tail end of the reduction process (see Figure 6), but the anodic current increased no further thereafter. This result is also consistent with the CVs, in that the PPy reduction is completed by -1.00 V, so that starting at more negative potentials does not lead to greater charge consumed upon oxidation. (Recall that the hydrolysis current was subtracted from the curves shown in Figure 8.) Further information on charge consumption during anodic stepping is presented in the Supporting Information.

The corresponding normalized curves are shown in Figure 8d. There was a smaller dependence of the speed on E_{ca} than on E_{an}, the current decaying somewhat more *slowly* as the pre-applied cathodic voltage was increased. This is surprising in light of the ESCR model: as the polymer becomes more reduced, the matrix becomes increasingly open, which one would expect to increase the subsequent oxidation speed. The $t_{0.5}$ and $t_{0.9}$ times for the anodic current are shown vs. E_{ca} in Figure 9b. (The two plots match up since the conditions on the right hand side of a) are identical to those on the left hand side of b): E_{ca} = -1.40 and E_{an} = +0.40 V.) The reaction speed only slows down with E_{ca} up to -1.0 V; beyond that, further increases in the cathodic voltage do not further slow the current decay by this measure. This plateau behavior is consistent with the

ESCR model: once the polymer matrix is fully open, ion transport out of the matrix upon subsequent oxidation is unaffected by the initial E_{ca}, and only depends on E_{an}.

To better understand these time dependences, we now quantify the decay using exponential curve fits.

3.3.2   Time Constants

It has consistently been observed (see for example [7]) that switching of a non-compacted film, as is done during this anodic step in PPy(DBS), gives rise to an exponentially decreasing current. The time constants for the anodic reaction, τ, determined by stretched exponential fits as defined in equation (5), are shown for all the data in Figure 10. Smaller values of τ correspond to faster switching.

The time constants τ are shown vs. the anodic potential in Figure 10a. (The curve for $E_{ca} = -1.40$ V having the black points with the dashed line corresponds to the CA series shown in Figure 8a and the results in Figure 9a.) The faster reaction rate, due to faster ion transport under higher fields, is reflected in all the curves by the decrease in τ with E_{an}. This decrease was more pronounced when stepping from the partially oxidized state at -0.7 V than when stepping from more negative initial cathodic potentials. The decrease in speed upon raising the cathodic potential from -0.7 to -1.0 is reflected in the rising positions of those curves.
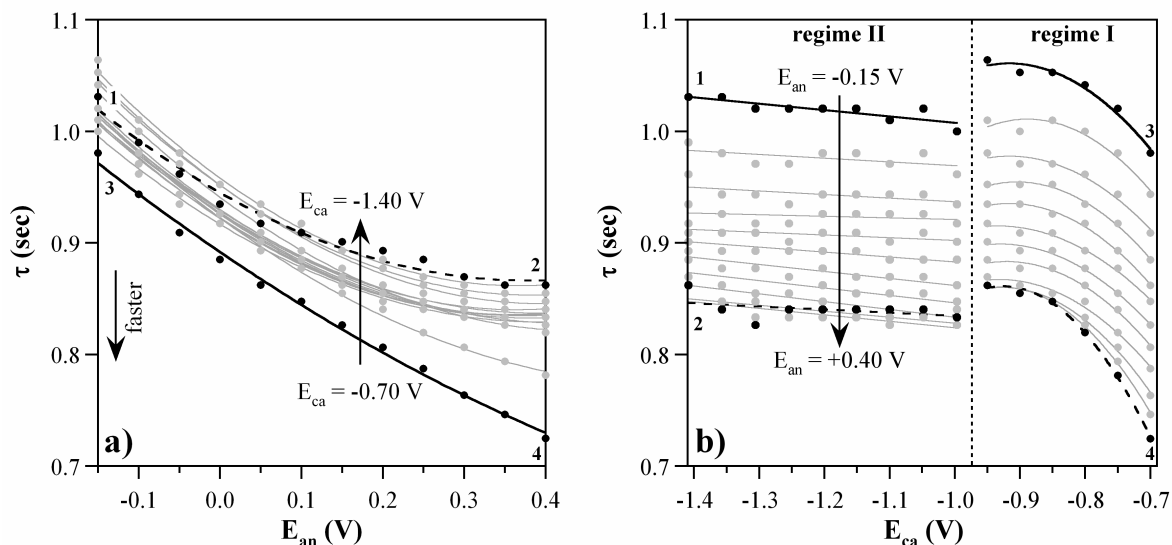
Figure 10. a) Anodic time constant τ as a function of E_{an} for different pre-applied cathodic potentials E_{ca}. Smaller τ indicates a faster reaction. b) τ plotted as a function of E_{ca} for different anodic potentials. The lines are guides for the eye. The labeled points 1-4 indicate how the two plots map one to another.

Figure 10b illustrates more clearly how the oxidation kinetics depended on E_{ca}, the cathodic potential that had been applied just before switching, for all the data. (Again, the black dashed line corresponds to the curves in Figure 8d and closely resembles the results in Figure 9b.) When τ is plotted as a function of E_{ca}, a two-regime behavior can be observed. (This is also seen in the charge, as shown in the Supporting Information.) In regime I, τ increased with E_{ca}, but in regime II, beyond -1 V, there was no further change. In regime I, larger cathodic potentials increase the reduction level of the polymer. The increase in τ might arise because switching from a more reduced state requires more charge to be exchanged (Figure 6 and Figure 8c) (it takes more time to move more charge into and through the polymer at the same E_{an}) and/or because of the higher electrical resistance of the more highly reduced state. The effect is greatest for high E_{an}, at which τ increased 19%, compared to 8% for the lowest E_{an}. The increase in τ

34

suggests that any benefit to the speed due to matrix opening between -0.7 V and -1.0 V (which would decrease τ by increasing the mobility and diffusivity of the ions) is more than offset by the increased resistivity. Beyond -1.0 V there is little effect on the subsequent anodic reaction rate from increasing E_{ca}, since the polymer is already fully reduced and changes no further.

3.3.3 Summary

To summarize the results in this section, the anodic currents were well described by simple stretched exponentials regardless of the initial and final voltages. Thus, as expected for a cation-transporting material, there was no manifestation of conformational relaxation since the matrix was transitioning from an open to a compacted state. The current magnitudes and decay times had a dependence on both initial and final voltages. Higher anodic potentials led to faster reactions (a decrease in response times of up to 50%), as would be expected simply on the basis of ion transport due to diffusion and drift under higher electric fields. The disadvantage of higher anodic voltages is that they lead to greater charge consumption, which means lower actuator efficiency. Interestingly, as the initial reduction level of the polymer was increased, the reaction slowed; beyond the fully reduced state, however, there was little further change in speed. Thus, there was no benefit due to starting the anodic step from an even more open initial matrix; rather, the disadvantage of the higher resistivity appears to be greater. It would be illuminating to perform analogous voltage stepping experiments with actuators to determine how the CA current and the movement are correlated.

3.4 Chronoamperometry: Cathodic Currents

We now turn to an examination of the cathodic currents, which are expected to reflect conformational relaxation since the polymer starts from a compacted state and must expand to allow cation ingress. As explained in section 2.2.2, because of the presence of shoulders the cathodic curves were analyzed in terms of both an exponential and a subtracted component. Results are first presented as a function of cathodic potential. In this first set of experiments, since the cathodic potential is varied, the results also reflect the effect of faster charge migration under higher electric fields. This is unavoidable: these effects cannot be separated in this type of experiment. However, in the last set of experiments (section 3.4.3), in which the time that the polymer is held at the anodic potential prior to switching is varied and the voltage endpoints are kept constant, these effects can be separated.

3.4.1 Role of Cathodic (Relaxation) Potential

The evolution of the cathodic CAs with increasingly cathodic potential E_{ca}, from -0.7 to -1.4 V, is shown in Figure 11a. All the currents reached a constant value before $t = 5$ seconds. As expected from the CV, the currents increased with E_{ca} up to $E_{ca} = -1.0$ V (gray lines), but increased little further for more negative potentials (black lines). In addition, with increasing cathodic potential a shoulder emerged and evolved, changing the shape of the overall curve. Again, the relative time responses are best seen by normalizing the curves (Figure 11b). Overall, the reaction increased in speed with E_{ca}.
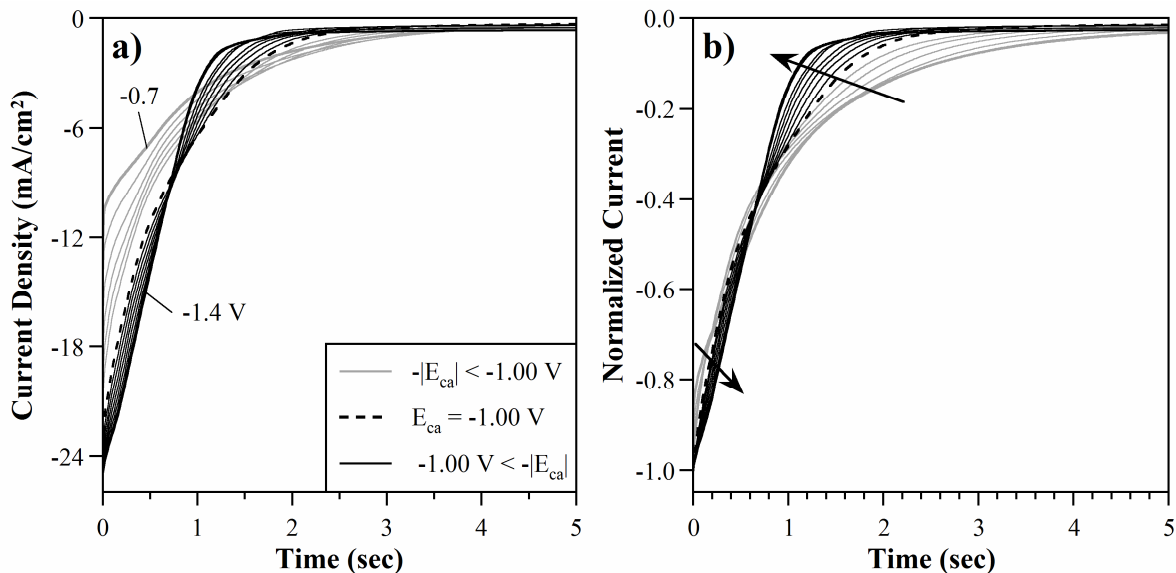
Figure 11. a) Cathodic chronoamperograms for a series of increasingly cathodic applied potentials, stepping from one anodic potential (+0.40 V held for 5 seconds). The arrows indicate increasing E_{ca}, with potentials less negative than -1 V indicated by gray lines, and those more negative by black lines. The first and last scans of the series are indicated by the heavier lines. b) The same data, normalized at $t = 0.0$ sec.

Figure 11b shows that for the cathodic step, as for the anodic step, one can increase the speed of the overall reaction by increasing the potential, but on this end one can do so *without* decreased efficiency: there was no increase in charge consumed between -1.0 V and -1.4 V (Figure 12). Most of the increase in speed comes from shortening the "tails" of the curves, which are much longer for smaller E_{ca}. The time $t_{0.9}$ required for the current to decay to 10% of its initial value is shown in Figure 13. With increasing cathodic potential, the cathodic reaction speeded up considerably, from 2.6 to 1.1 second based on this measure. This shows a much stronger dependence on the driving voltage than the anodic current did on the anodic voltage (raising E_{an} from -0.15 to 0.4 produced a drop of only 0.5 seconds). This result is consistent with models of ion transport based on diffusion and drift [27,46,48], which show that reduction is dominated by

ion migration in the polymer, and is thus very responsive to changes in voltage, while during

oxidation ion transport in the polymer is instead dominated by diffusion, and is thus only

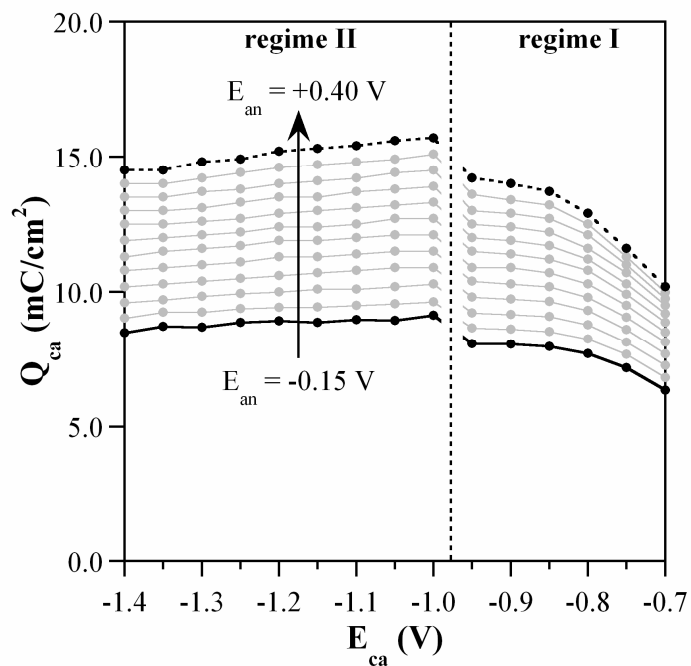indirectly affected by changes in voltage.

Figure 12. Absolute value of the total cathodic charge as a function of cathodic potential. In regime I, the reduction level of the polymer is increasing, while in regime II it has reached the fully reduced state and changes no further.
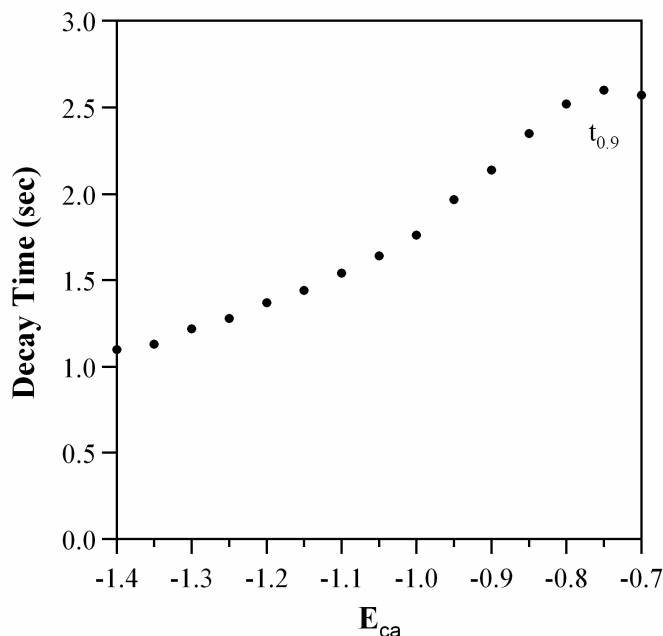
Figure 13. Time required for the cathodic current to drop to 10% of its initial value as a function of E_{ca}.

To better understand the evolution of the CAs, exponential curve fits and the ESCR peaks that resulted from subtracting those fits from the data are shown for two different E_{ca} in Figure 14a. Only those curves starting from various anodic potentials and stepping to $E_{ca} = -0.70, -0.75,$ and -0.80 V could be well fit with an exponential alone: note that the subtracted component of the $E_{ca} = -0.70$ V curve in Figure 14a is negligible. All the other curves yielded ESCR peaks of increasing size as the cathodic potential increased, as illustrated in Figure 14b, indicating that a greater number of ions encountered compacted material. In addition, the ESCR peak position t_{ESCR} moved to shorter times, indicating that conformational relaxation occurred more quickly. Note that as E_{ca} increased, Γ_1 approached zero, so that for $E_{ca} > -1.05$ V only the single point $t = 0.2$ was fit in front of the ESCR peak. There was, however, a reasonably long stretch Γ_2 from which to obtain τ. Nevertheless, there may be some uncertainty in τ for $E_{ca} > -1.05$ V. The fits are further discussed in the Supporting Information.
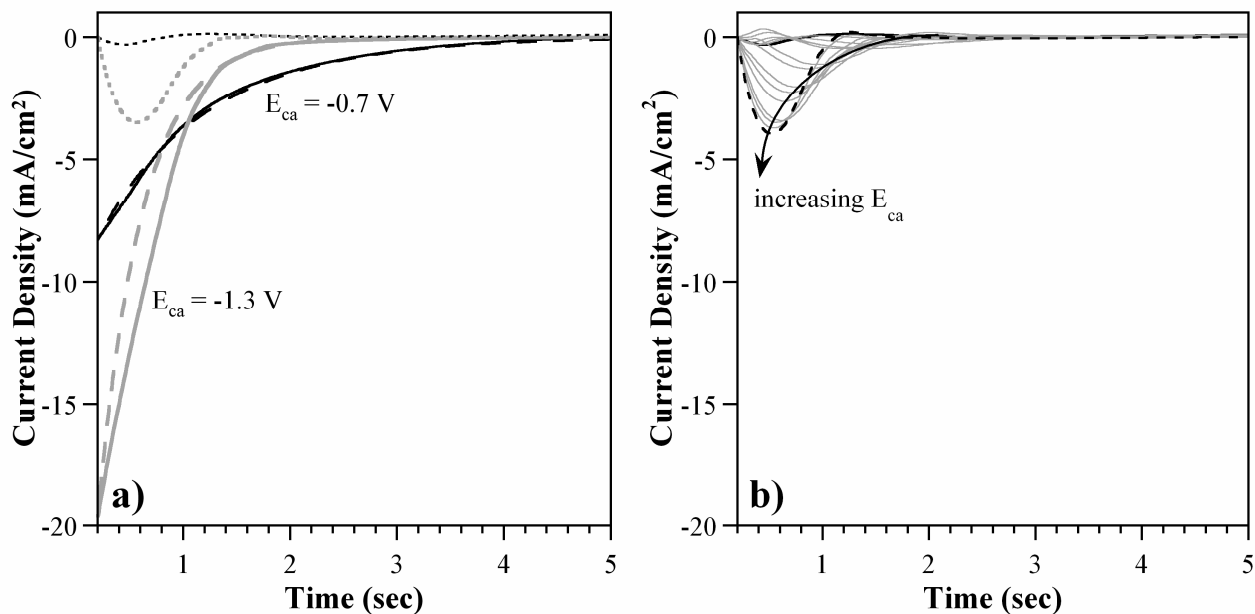
Figure 14. a) Corrected CA data (solid curves), exponential fits (dashed lines), and subtracted (ESCR) components (dotted lines) for a low (black) and a high (gray) cathodic potential, both stepping from E_{an} = +0.40V. b) ESCR components for the whole range of increasingly cathodic potentials, again stepping from E_{an} = +0.40V. The curves for E_{ca} = -0.7 V (solid line) and -1.30 V (dashed line), shown in panel a), are highlighted in black.

The fact that more of the current was affected by conformation relaxation as E_{ca} increased, but that the relaxation occurred more quickly might seem contradictory. However, as E_{ca} goes up, the ions move more quickly (due to faster migration). It is possible that a greater number of them therefore enter the polymer before it has had a chance to relax, and must then wait for ESCR before they can move further, thus contributing to the peak. At lower E_{ca}, on the other hand, the relaxation may be largely complete before the bulk of the ions arrive. At the same time, higher E_{ca} provides more energy for the conformational relaxation, speeding it up.

At this point, it is important to note that it is not entirely clear how the currents in the cyclic voltammograms correspond with those in the chronoamperograms. Specifically, it is not known if 1) the ESCR peak is associated with Gaussian 1 and the exponential peak is associated with Gaussian 2 and the so-called capacitive current, or 2) if instead all the current components identified on the CV contribute to both the exponential decay and the ESCR peaks. Case 1 is more likely because the charge under Gaussian 1 and the ESCR peak are of comparable magnitude and because it is reasonable to suppose that ion transport associated with strain requires chain conformation (strain has previously been shown to be associated with Gaussian 1 [28]). Until comparable experiments are done with actuators and/or electrochromic devices, the significance of the exponential current cannot be determined. Such experiments will, however, be complicated by the two types of cation transport that occur simultaneously in PPy(DBS): fast lateral ion transport from the edges of the film to the center (due to ion transport parallel to the PPy chains along the DBS lamellae) and slower vertical ion transport from the surface toward the electrode (due to ion transport through the PPy chains) [49]. In fact, it is also possible that the lateral transport is associated with the exponential current component, and that the vertical transport is associated with the ESCR peak. These questions must be deferred for the present, but the chronoamperograms will be thoroughly characterized below.

The following sections examine the speed and magnitude of the exponential decay and ESCR processes in more detail, but it is clear from Figure 11b and Figure 14b that both become faster with E_{ca}. This is consistent both with greater velocities of charge migration into the polymer under higher cathodic voltages, as well as with increasingly fast polymer relaxation, as expected from the ESCR model.

In the following analysis of the ESCR processes, in some cases only data obtained from stepping to cathodic potentials greater than -1.0 V are used, since the film is not fully reduced until that point. Steps to less negative voltages (gray lines in Figure 11) do not take the polymer to the same state, and therefore the results cannot be fairly compared. In examining the exponential decay processes, all the data have been shown, but the difference in final states of the polymer should be borne in mind.

3.4.1.1 *Exponential Curve Time Constant*

To quantify the increase in speed of the exponential decay component of the current during reduction, the log of the time constants τ (see equation (6)) of the exponential fits were plotted vs. E_{ca} (Figure 15). (Additional plots are shown in the Supporting Information.) The time constant of the exponential process decreased strongly with E_{ca} (i.e., with increasingly negative E_{ca}), consistent with both the ESCR model and with faster migration under higher electric fields. The τ also depended on the previously applied E_{an}, increasing somewhat as E_{an} was raised (indicated by the arrow). This is discussed below.
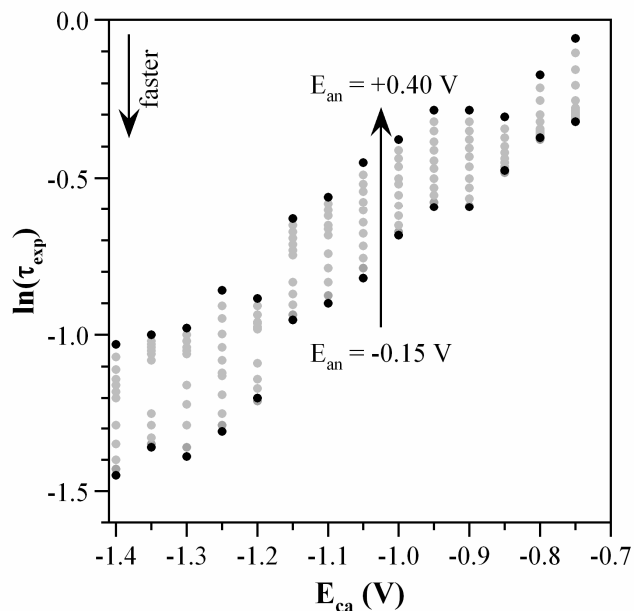
Figure 15. Natural logarithm of the time constants τ for the exponential curve fits to the cathodic CAs, plotted as a function of cathodic potential upon stepping from different pre-applied anodic potentials.

3.4.1.2 *ESCR Peak Position*

We now turn to the "subtracted" peak. As shown in Figure 14b, the ESCR curve peaked sooner with increasing cathodic potential. The ESCR model (equation (4)) predicts that t_{ESCR}, the peak time, should have a logarithmic dependence on E_{ca}. It does, as shown in Figure 16a. The good fits (correlation coefficients R were between 0.986 and 0.996) indicate that conformational relaxation kinetics control the reaction process represented by this current component, with faster conformational relaxation under larger cathodic overpotentials.

The intercepts of the lines in Figure 16a increased with E_{an}, showing that the initial state of the polymer affects the speed of ESCR, with higher E_{an} producing a more compact matrix, and thus

increasingly time-delayed peaks. A greater amount of energy is therefore required to open the structure in the same time.
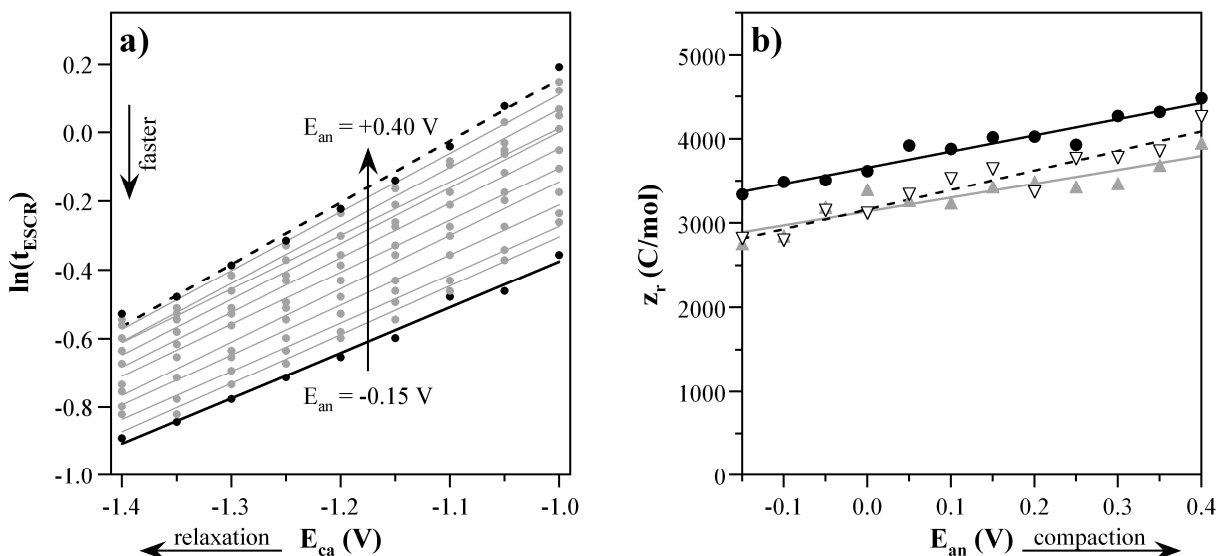

Figure 16. a) Log of the ESCR peak position as a function of cathodic potential for different anodic potentials. b) The charge z_r required to relax one mole of polymer segments, with the filled black symbols showing the data obtained from panel a) and the other two symbols showing data obtained from the other two data sets. (Correlation coefficients R were 0.968 for the filled circles, 0.955 for the empty triangles (dashed black line), and 0.914 for the gray triangles (solid gray line).)

The slopes of the lines in Figure 16a were used to obtain the constants z_r, which quantify the charge required to relax one mole of polymer segments from equation (4), shown again here for ease of understanding:

(4) $\ln(t_{ESCR}) = C' - z_r\eta_r/RT.$

Correlating equation (4) with Figure 16a, C' represents the y-intercept of the lines, $\eta_r = (E_0 - E_r)$ represents the independent variable (on the x-axis, where $E_r = E_{ca}$ is the cathodic reduction potential), and z_r/RT represents the slope of the lines. E_0 is the potential at which reduction

begins. Based on the total current in the cyclic voltammogram in Figure 6, $E_0 = -0.2$ V, but based on Gaussian 1, $E_0 = -0.5$ V. The latter value agrees with the one previously observed for the onset of higher lateral mobility in PPy(DBS) due to matrix opening (see Figure 26 in [28]). The value chosen for E_0 does not affect the calculation of z_r. The ideal gas constant R and the temperature T were taken as 8.314 J/(K*mol) and 300 K, respectively, giving $RT = 2494$ J/mol. Under these assumptions, z_r was calculated by multiplying the slope of the lines by RT.[*]

The values of z_r found from Figure 16a and from the other two sets of data are plotted as a function of E_{an} in Figure 16b. They begin at 2800-3500 C/mol for initial $E_{an} = -0.15$ V and increase to 3800-4500 C/mol for initial $E_{an} = 0.40$ V. Increasing z_r with increasing compaction overpotentials was expected from the model and from prior experimental results with other conjugated polymers. As has been found previously, the higher the degree of closure of the matrix, the more sensitive the opening of the structure is to the electric fields [5].

3.4.2 Role of Anodic (Compaction) Potential

We now examine the effect of the anodic (compaction) potential on the subsequent cathodic chronoamperograms, which are expected to be strongly influenced by ESCR. A series of chronoamperograms was taken upon stepping to fixed cathodic potentials from different initial anodic potentials; each potential, anodic and cathodic, was held for 5 seconds (Figure 4). As shown in Figure 17a for the fixed E_{ca} of -1.40 V, with increasing E_{an} the cathodic current curves shifted to the right (longer reaction completion times) and slightly down (somewhat higher initial

---

[*] For the purpose of the calculation, the signs of the slopes were reversed because of the way the compaction potential was plotted in Figure 16a, with increasing overpotentials to the left, instead of to the right as in anion-transporters.

currents). The higher currents were expected due to the greater quantity of charge that must be exchanged when starting at higher E_{an}, as seen in the cyclic voltammograms.
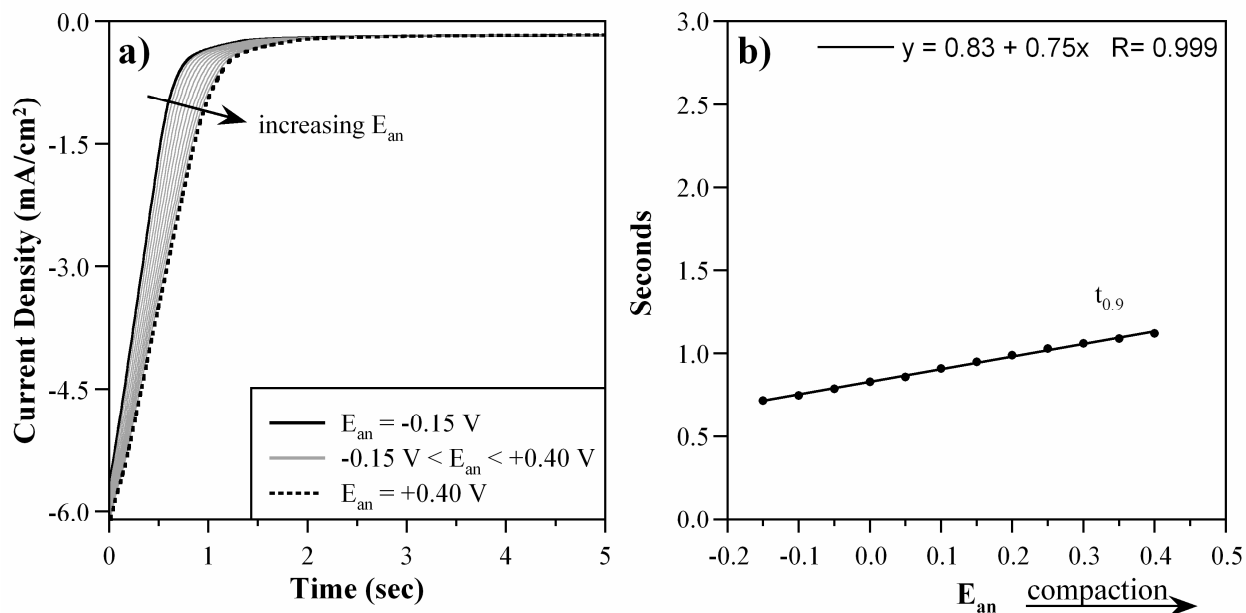

Figure 17. a) Cathodic chronoamperograms for a series of pre-applied anodic potentials E_{an} upon stepping to one cathodic potential (-1.40 V vs. Ag/AgCl). b) Time required to reduce the cathodic current to 10% of its initial value as a function of E_{an}.

Using the time for the current to decay to 10% of its initial value as a measure of the reaction time, the time is found to be linear with increasing E_{an}. Thus, while increasing E_{an} causes the anodic step go faster (by 0.5 seconds in going from -0.15 to +0.40 V), it also causes the subsequent cathodic step to go slower (by 0.4 seconds over the same range). The benefits of a faster anodic step must therefore be weighed against the detriment of an almost equally slower cathodic step.

Exponential curve fits and the ESCR peaks that resulted from subtracting those fits from the data are shown for a low and a high E_{an} in Figure 18a. Like the CA curves from which they were derived, the exponential fits decayed more slowly as E_{an} was increased (shown in the Supporting Information). Figure 18b shows that the ESCR peaks increased in magnitude (more of the polymer was compacted, so more of the current was affected), and also that the positions of the peak shifted to longer times (ion transport must wait longer for matrix relaxation to occur). These results lend additional support to the hypothesis that these peaks arise from conformational relaxation processes. We now examine these time dependences in more detail.
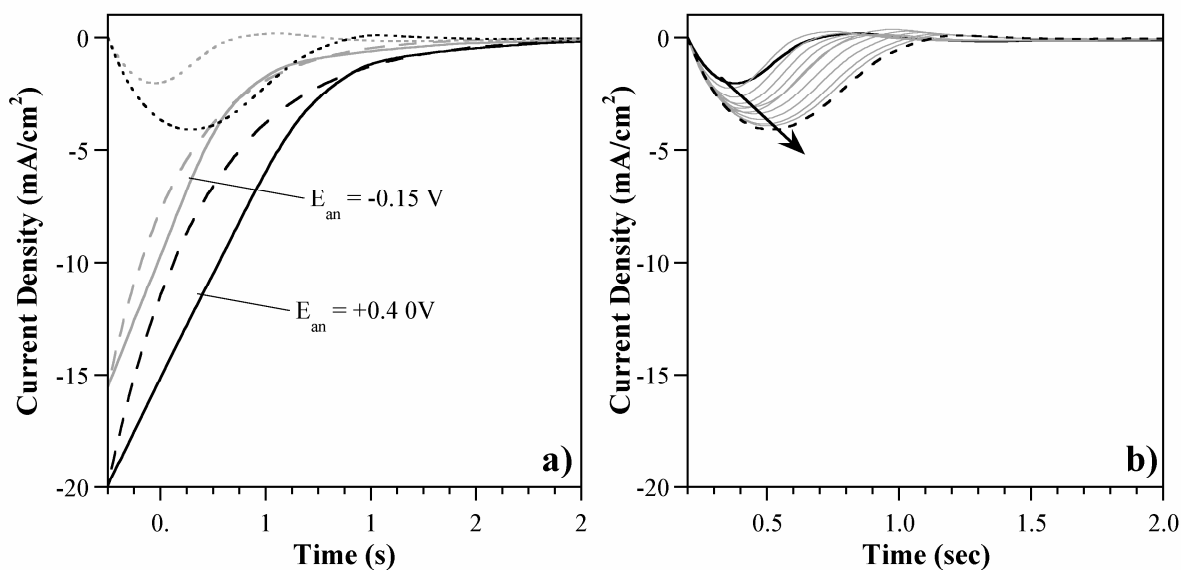

Figure 18. a) Exponential (dashed lines) and ESCR (dotted lines) components of the cathodic current (solid lines) upon stepping to E_{ca} = -1.40 V from high and low initial anodic potentials. b) ESCR components for the whole range of increasingly anodic pre-potentials, again stepping to E_{ca} = -1.40 V. The highlighted curves for E_{an} = -0.15 V (solid black line) and +0.4 V (dashed black line) were shown in panel (a).

3.4.2.1 Exponential Curve Time Constant

The logs of the time constants obtained from the exponential fits are plotted as a function of E_{an} in Figure 19. For all E_{ca}, the response times increased slightly with anodic potential, E_{an}. The reasons for this are not yet clear, since the exponential current is presumably due to unimpeded ion transport in an open matrix. As E_{ca} was increased, the lines moved downward, reflecting the faster cathodic response under more negative voltages that was detailed in the previous section (Figure 15).
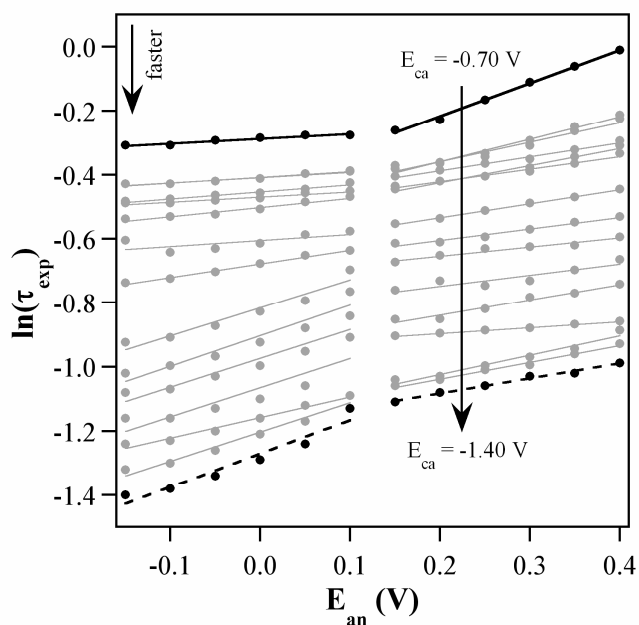

Figure 19. Cathodic exponential time constants as a function of the pre-applied anodic potential upon stepping to different cathodic potentials.

The increase in τ_{exp} occurred even for E_{ca} = -0.7, -0.75, and -0.80, for which there was no ESCR peak. In addition, the increase was seen in all three data sets (shown in the Supporting

Information). This is therefore a real effect. There was a change in slope at low E_{an} starting at approximately $E_{ca} = $ -1.00 V, corresponding to when the polymer becomes fully reduced and the subtracted curves become significant compared to the noise. At high E_{an}, the slopes remained essentially constant.

For $E_{ca} = $ -0.7, -0.75, and -0.80, the τ_{exp} were obtained by fitting the entire CA curve, since there was no ESCR peak at those low cathodic potentials; confidence in these values can therefore be high. One can also have confidence in the time constants for $E_{ca} = $ -0.85 through -1.10 V, for which the curve fits were able to use some portion of the beginning of the curve ($\Gamma_1 \neq 0$). The τ_{exp} for E_{ca} more negative than -1.10 V, obtained from curve fits for which $\Gamma_1 = 0$, were consistent with the other lines, so it is likely that these results are also reliable.

If the exponential is due to pure diffusion and migration of ions in an open matrix, one would not expect a dependence on E_{an}. Perhaps this ion transport process reflects more compact chain conformations through a slowing of the ions as a result of increased scattering. It is important, however, to recall that in these experiments, effects due to changes in migration, conformation, electrical conductivity, and amount of charge exchanged cannot be neatly separated. Another possibility is that starting from higher anodic potentials results in slower switching since it requires more charge to be exchanged (see the CV in Figure 6), or that this increment of charge goes to different types of sites in the polymer. Resolving this question would require further studies outside the scope of this paper.

3.4.2.2 ESCR Peak Position

The behavior of the subtracted peak as a function of the compaction potential E_{an} is now

discussed. For E_{ca} that were less negative than -0.80 V, no clear "subtracted" curve existed,

regardless of the initial E_{an} that was applied, perhaps because chain relaxation is not rate-limiting

at those potentials (for example, because ion migration velocities are rate-limiting). It is also

possible that there were no ESCR peaks because these overpotentials are not high enough to

reduce the fraction of the material that has been compacted. (Under these E_{ca}, the polymer is not

completely reduced, as seen in the cyclic voltammograms and reflected in the lower charge

exchanged.) It would be consistent with the ESCR model to postulate that the compacted

material requires higher overpotentials η_c to be reduced. This would also be consistent with a

relationship between Gauss 1 (Figure 6b) and the ESCR peak. If no electrons are added to the

compacted material because higher energies are required to put the electrons there than onto

noncompacted material, then the cations have no reason to enter the compacted material, and no

ESCR peak would be produced.

In the plots presented below, even though ESCR peaks existed for E_{ca} = -0.85, -0.90, and -0.95

V, only data taken at or below -1.0 V were used so that comparisons were made of the polymer

in the same fully reduced final state. This allows us to examine only ESCR processes, rather

than a mixture of these with reduction processes.

According to equation (4), a log dependence of t_{ESCR} on E_{an} is expected. Figure 20a shows that

this was the case: increasing anodic pre-potentials resulted in logarithmically longer t_{ESCR}. The

decrease in peak time with cathodic potential E_{ca} that is seen here as a downward shift of the lines was previously detailed in section 3.4.1.2.
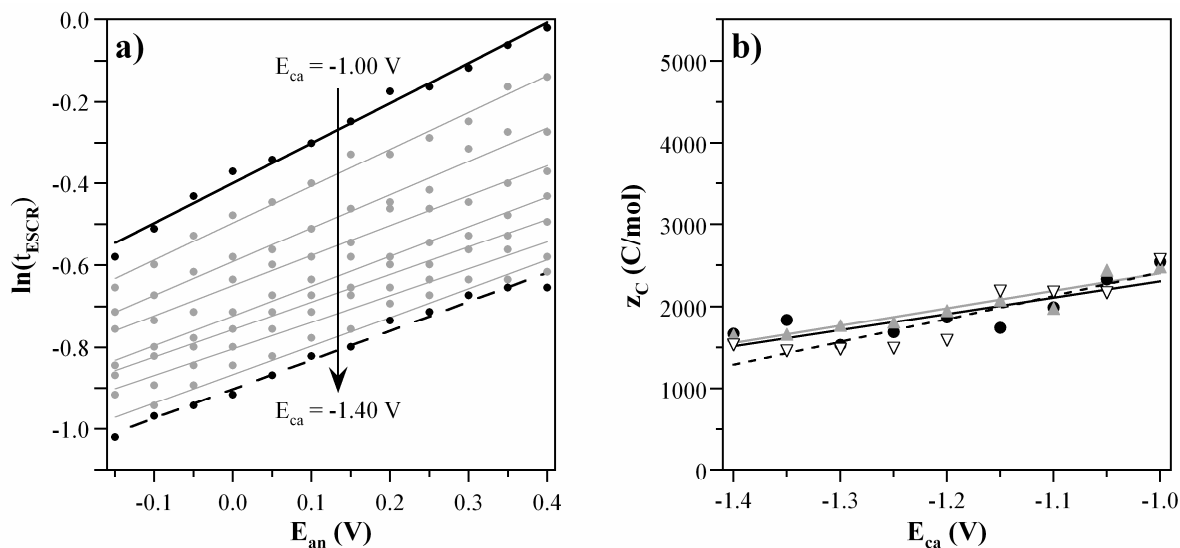

Figure 20. a) ESCR peak position as a function of pre-applied anodic potential for a series of cathodic potentials. b) The charge z_c required to compact one mole of polymer segments, with the filled black symbols showing the data obtained from panel a) and the other two symbols showing data obtained from the other two data sets.

The slopes of the curves in Figure 20a were used to calculate z_c, the amount of charge required to *compact* one mole of polymeric segments, analogously to the calculation of z_r in section 3.4.1.2. The values of z_c are shown as a function of cathodic potential in Figure 20b.

The values of z_c are less than the values of z_r (compare Figure 16b). This has usually been the case in other polymers as well. As shown in reference [17], the size of z_c and z_r are inversely linked by the strength of the interaction of the solvent with the polymer. A smaller z_c than z_r shows that there are strong polymer-solvent interactions, favoring matrix opening, so that larger

compaction overpotentials are needed to close the structure (smaller z_c), and smaller relaxation

overpotentials are needed to open it to the same degree (larger z_r) [17]. This becomes clear from

looking at equation (2): $\Delta H \sim z_c \eta_c - z_r \eta_r$. Achieving the same ΔH given a larger z requires a

smaller η.

The compaction constant z_c decreased with increasingly cathodic potentials, meaning that larger

compaction overpotentials are needed to close the structure to the same extent. The reason for

this is not clear, since within regime II the polymer matrix was not thought to change (Figure

10).

3.4.3   Role of Anodic Holding Time

In the previous sections, the direct role of the voltage on ion transport via migration could not be

neatly separated from the indirect role of the voltage on ion transport via electrochemically

stimulated chain relaxation. There is, however, a set of experiments that can successfully

separate migration and ESCR effects: changing the holding or "wait time" t_{wait}, i.e. the time for

which the polymer is held in the oxidized state before the cathodic step is applied. The longer

the holding time, the more compacted the matrix becomes. Since the starting and ending

potentials are the same, the migration and diffusion forces are the same. Thus, any change in the

chronoamperograms can only be due to compaction and relaxation of the polymer.

The potential was held at 0.0 V to compact the polymer for times between 1 second and 1000 seconds, and then it was stepped to -1.0 V and held for 20 seconds. To completely "erase" the memory, two CVs were done before proceeding to the next oxidation step.

Figure 21 shows the cathodic CAs as a function of holding time t_{wait}. They move toward longer times and greater total consumed charge with increasing holding time, although, interestingly, the initial current density remained unchanged.
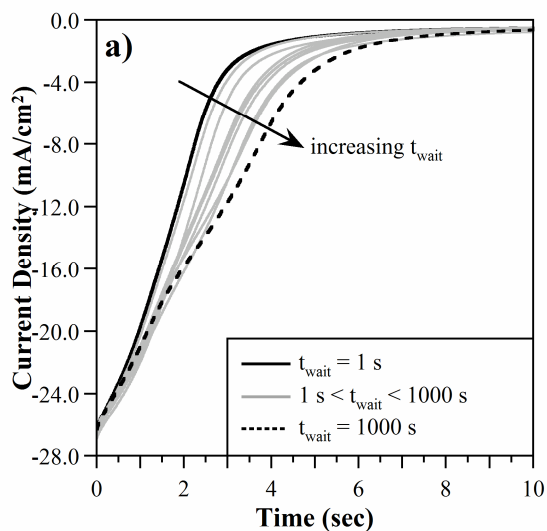

Figure 21. Cathodic CAs to -1.0 V after holding at 0.0 V for varying times.

It was not possible to accurately determine the exponential time constants for the longer holding times because of the large size and long duration of the ESCR peak. Therefore, a single time constant τ, the one that best fit the 1 second holding time CA (which had the smallest ESCR peak, and thus the most reliable fit), was used for the exponential fits for all of these CAs. This approach assumes that the exponential current decay is unaffected by ESCR processes. If this

current component is due to unimpeded diffusion/drift in an open matrix, then this assumption is reasonable. However, without accurate fits this assumption cannot be tested.

The exponential fit and the ESCR peaks for two holding times are shown in Figure 22a, while Figure 22b shows the entire series of ESCR peaks obtained at all the holding times. These peaks grew in size, and shifted to longer times, as the holding time was increased, consistent with the ESCR theory. In fact, this behavior cannot be accounted for in any other way.
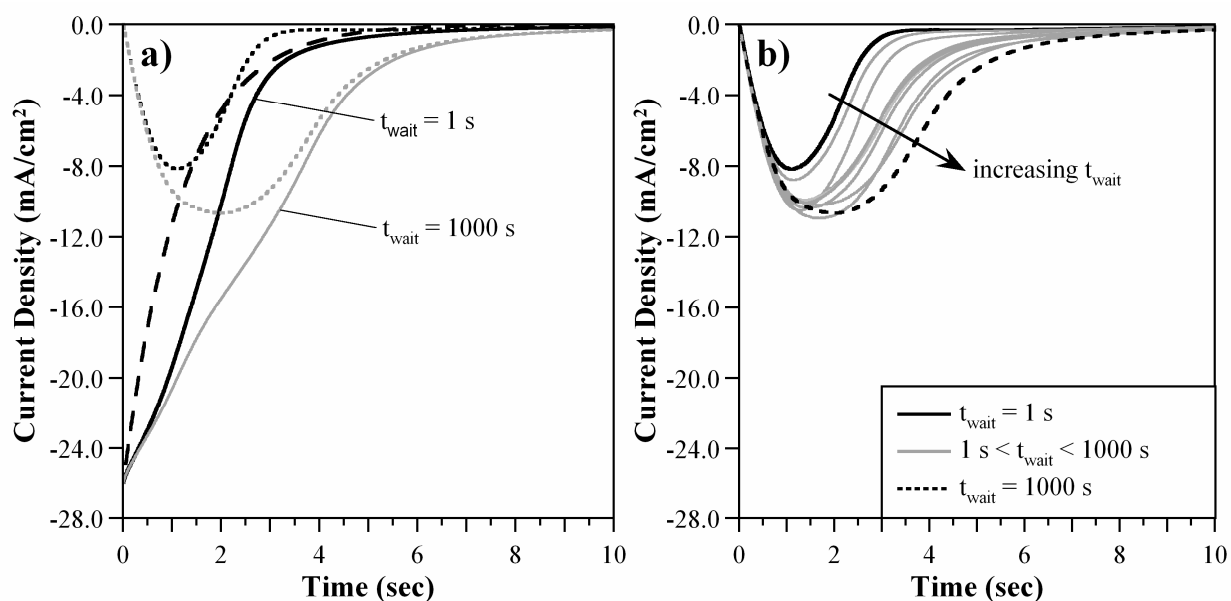

Figure 22. a) Curve fits to cathodic CAs at two different anodic holding times: 1 second (black lines) and 1000 seconds (gray lines). Cathodic data, the exponential fit (the same for all curves), and the ESCR peaks are denoted by solid, dashed, and dotted lines, respectively. b) The resulting ESCR peaks for the whole series of holding times, with the two cases in panel (a) highlighted in black.

It may seem surprising that the total charge consumed during reduction increased. Since this shows that a greater number of cations are pulled into the polymer after longer holding times,

cations must continue to be gradually expelled over time as the polymer is held in the oxidized state, bringing the film to a higher oxidation level. Again, experiments with actuators would be informative: is there a positional drift when the polymer is held in the oxidized state? (Pei's work on PPy(DBS) bilayer actuators examined curvature drift over time in the *reduced* state [50].)

3.4.3.1 *ESCR Peak Position*

According to equation (8),

(8) $\qquad ln(t_{ESCR}) = C + A\, ln(t_{wait})$, equivalent to $t_{ESCR} = c\left(t_{wait} \right)^{A}$,

where C and c are constants, so the log of the ESCR peak time should depend logarithmically on the anodic holding time [12]; this is shown in Figure 23. The relationship of $ln(t_{ESCR})$ with $ln(t_{wait})$ is indeed approximately linear. (Alternatively, plotting t_{ESCR} vs. t_{wait} gives $y = 1.2x^{0.065}$ with R = 0.86. This power law allows the data to be interpreted more easily for actuator control.) With this final piece of evidence, we can firmly conclude that the ESCR peak is definitely due to ESCR processes.
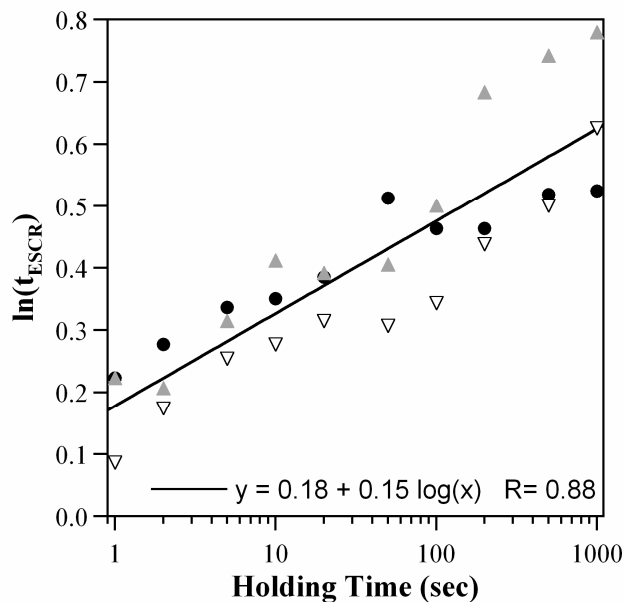
Figure 23. ESCR peak position as a function of anodic holding time, with the empty triangles showing the data obtained from Figure 22, and the other two symbols showing data obtained from the other two data sets. The line shows the best fit to all three sets of data.

3.4.3.2 *Charge*

Figure 21 showed that the total charge increased with the holding time. Figure 24 shows that the charge in fact increased logarithmically with holding time, just as the peak position did.[*]

---

[*] Given the fixed exponential fit for all the curves, when the total charge q_{tot} was split into exponential and ESCR components, only the ESCR charge q_{ESCR} could increase with holding time. The small decrease in q_{exp} with holding time is due to the fact that the charge integration started at $t = 0.2$ rather than $t = 0$ seconds.
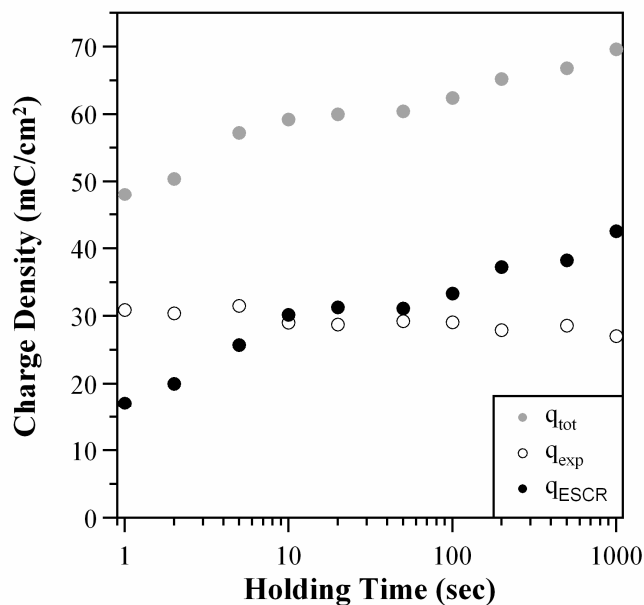
Figure 24. Absolute magnitude of the cathodic charge densities as a function of holding time: total (gray), exponential (empty), and ESCR (black) charge.

4 DISCUSSION AND CONCLUSIONS

The presence of the shoulder on the decaying cathodic current, the voltage and holding time dependence of this shoulder, and the absence of a similar shoulder on the decaying anodic current are strong evidence for electrochemically stimulated conformational relaxation in PPy(DBS). The shoulder occurs sooner when the cathodic potential E_{ca} is increased, with a logarithmic dependence of the peak time on E_{ca}, consistent with an interpretation that greater cathodic potentials provide more energy for conformational relaxation. The shoulder occurs later as the anodic potential E_{an} is raised, again with a logarithmic dependence of peak time on E_{an}, consistent with an interpretation that greater anodic potentials produce greater compaction. Finally, the shoulder occurs later the longer E_{an} is held prior to the cathodic step, with a power

law dependence of the peak time on the holding time, consistent with an interpretation that compaction gradually continues in the anodic state. These matrix effects on ion transport, while not as significant as they are in anion-transporting materials, nevertheless need to be considered in any actuator control algorithms, since they give the material a "memory".

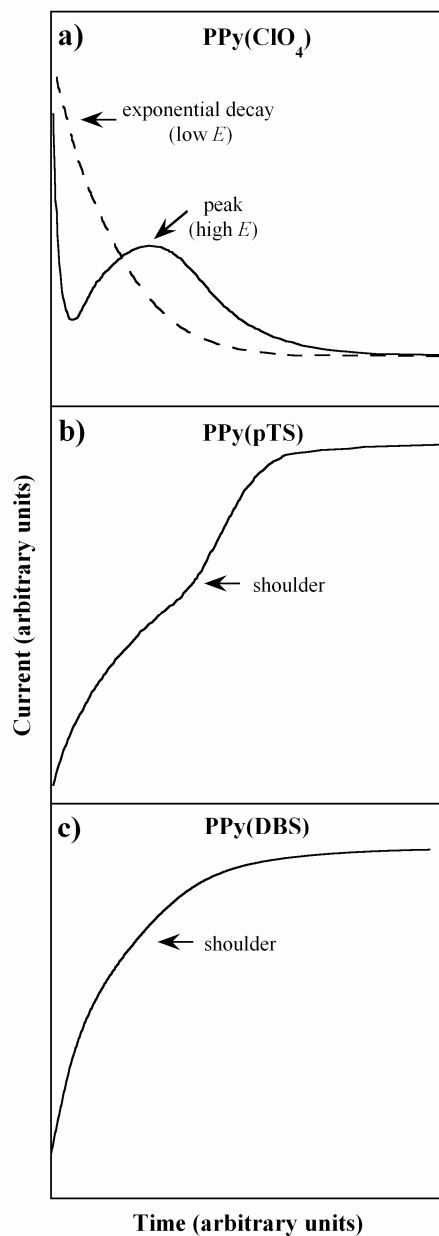**Figure 25.** Comparison of the shapes of the chronoamperometric peaks in (a) a typical anion-transporting system, PPy(ClO$_4$) cycled in ACN/LiClO$_4$ [6], and in two cation-transporting systems: (b) PPy(pTS) cycled in PC/LiClO$_4$ [19] and (c) PPy(DBS) cycled in aqueous NaDBS. Currents and times are not directly comparable because the overpotentials differed, the films varied in thickness, and different electrolytes were used.

As is now clear from examining two cation-transporting systems, PPy(pTS) and PPy(DBS), conformational relaxation plays a much smaller role as a rate-limiting step than it does in anion-transporting polymers (Figure 25). In the latter, the matrix can be compacted to such an extent that switching of every part of the film is delayed until matrix relaxation begins, as evidenced by a single peak in the chronoamperogram (Figure 25a). In the absence of compaction, the chronoamperogram shows only an exponential decay (Figure 25a). On the other hand, in the two cation-transporters, even at their most compacted, ESCR affects only a fraction of the charge (20% in PPy(DBS)), and the remaining charge flows freely, as evidenced by the large exponential decay component and the small ESCR peak component. One can therefore conclude that the cation-transporting systems cannot be compacted to the same extent as the anion-transporters.

The inability to fully compact the cation-transporting polymers is most likely the result of the ions that are always present, in both oxidized and reduced states, and the accompanying water (as illustrated in Figure 3). Prior work on PPy(DBS) has shown that upon the first-ever reduction of the film, the out-of-plane volume increases approximately 60% as cations and water are pulled into polymer for the first time [28,31,51] (depending on the cation; these values are for Na^+ [52]). Upon re-oxidation, however, the film does not contract all the way back to its original thickness: there is a semi-permanent increase of ~25% due to ions and water that remain in the film. Thereafter, the reversible volume change upon redox cycling is ~30%, based on the new oxidized film thickness.

One could make the argument, therefore, that cation-transporting systems are better suited for actuators with respect to speed and control. Since the switching is less hindered by conformational relaxation, the polymers have less of a memory and should be easier to control. We emphasize, however, that this conclusion is based solely on the chronoamperograms. Until analogous studies are done with actuators, measuring the in-plane and out-of-plane volume change as a function of compaction potential and wait time, it is unclear whether the small fraction of charge affected by ESCR is the fraction that is critical for actuation. Recall that the amount of charge in Gaussian 1, known from prior work to be associated with actuation and with color change, is of comparable magnitude to the ESCR peak. Further, given that actuation is due to the creation of free volume in the polymer, it would be reasonable to suppose that the ESCR peak current is associated with actuation. The unhindered ion transport represented by the exponential decay component, if it is unassociated with the creation of free volume, may just represent lost actuator efficiency (defined as the fraction of electrical energy converted to mechanical energy) due to ion transport through already-open regions of the polymer matrix. one of the next questions to be answered, therefore, is "What is the role of the charge consumed in the exponential decay?" As pointed out above, this is still unknown. From the point of view of actuator control, answering the question, which cannot be done with the data presented here, of whether the ESCR peak is associated with Gaussian 1 is quite important. If that is the case, then it would explain the time delay in actuation that has been reported between switching the voltage and the commencement of movement. Also, it would demonstrate to what extent movement can be speeded up by applying higher voltages, and whether movement is correlated with the position of t_{ESCR}.

ACKNOWLEDGMENTS

REFERENCES

1.   C. Lopez, M. F. M. Viegas, G. Bidan, and E. Vieil, "Comparison of ion exchange properties of polypyrrole with and without immobilized dopants by optical beam deflection," Synth. Met., 63 (1)**,** 73-78 (1994).

2.   Y.-J. Qiu and J. R. Reynolds, "Dopant anion controlled ion transport behavior of polypyrrole," Polym. Eng. Sci., 31 (6)**,** 417-421 (1991).

3.   E. W. H. Jager, E. Smela, and O. Inganas, "Microfabricating Conjugated Polymer Actuators," Science, 290**,** 1540-1545 (2000).

4.   T. Shimidzu, A. Ohtani, T. Iyoda, and K. Honda, "Charge-controllable polypyrrole/polyelectrolyte composite membranes. Part II. Effect of incorporated anion size on the electrochemical oxidation-reduction process," J. Electroanal. Chem., 224**,** 123-135 (1987).

5.   T. F. Otero, H. Grande, and J. Rodriguez, "Influence of the counterion size on the rate of electrochemical relaxation in polypyrrole," Synth. Met., 83**,** 205 (1996).

6.   T. F. Otero, H. Grande, and J. Rodriguez, "Reinterpretation of Polypyrrole Electrochemistry after Consideration of Conformational Relaxation Processes," J Phys Chem B, 101**,** 3688-3697 (1997).

7.   T. F. Otero and I. Boyano, "Comparative Study of Conducting Polymers by the ESCR Model," J Phys Chem B, 107**,** 6730-6738 (2003).

8.   T. F. Otero and I. Boyano, "Potentiostatic Oxidation of Polyaniline under Conformational Relaxation Control: Experimental and Theoretical Study," J Phys Chem B, 107**,** 4269-4276 (2003).

9.   T. F. Otero, H. Grande, and J. Rodriguez, "Conformational relaxation during polypyrrole oxidation: from experiment to theory," Electrochim. Acta, 41 (11/12)**,** 1863-1869 (1996).

10. T. F. Otero, H. Grande, and J. Rodriguez, "Electrochemical oxidation of polypyrrole under conformational relaxation control. Electrochemical relaxation model," Synth. Met., 76**,** 285 (1996).

11. T. F. Otero, H. Grande, and J. Rodriguez, "A conformational relaxation approach to polypyrrole voltammetry," Synth. Met., 85**,** 1077 (1997).

12. H. Grande and T. F. Otero, "Conformational movements explain logarithic relaxation in conducting polymers," Electrochim. Acta, 44**,** 1893-1900 (1999).

13. C. Odin and M. Nechtschein, "Slow relaxation in conducting polymers," Phys. Rev. Lett., 67 (9)**,** 1114-1117 (1991).

14. C. Odin and M. Nechtschein, "Slow Relaxation in Conducting Polymers - Influence of the Wait Potential," Synth. Met., 55 (2-3)**,** 1287-1292 (1993).

15. T. F. Otero and H. Grande, "Thermally enhanced conformational relaxation during electrochemical oxidation of polypyrrole," Electroanal. Chem., 414**,** 171 (1996).

16. T. F. Otero, M. T. Cortes, and I. Boyano, "Molar enthalpy of the polypyrrole electrochemistry," J Electroanalytical Chem, 562**,** 161-165 (2004).

17. H. Grande, T. F. Otero, and I. Cantero, "Conformational relaxation in conducting polymers: effect of polymer-solvent interactions," J. Non-Cryst. Solids, 235**,** 619-622 (1998).

18. T. F. Otero, M. Marquez, and I. J. Suarez, "Polypyrrole: Diffusion coefficients and degradation by overoxidation," J. Phys. Chem. B, 108 (39)**,** 15429-15433 (2004).

19. T. F. Otero and J. Padilla, "Anodic shrinking and compaction of polypyrrole blend: electrochemical reduction under conformational relaxation kinetic control," Journal of Electroanalytical Chemistry, 561**,** 167-171 (2004).

20. T. F. Otero and M. T. Cortés, "Artificial muscles with tactile sensitivity," Adv. Mater., 15 (4)**,** 279-282 (2003).

21. T. F. Otero and M. T. Cortes Montanes, "Characterization of triple layers," Proc. SPIE's 8th Int. Symp. Smart Struc. Mater., Electroactive Polymer Actuators and Devices (EAPAD), Newport Beach, CA, vol. 4329, edited by Y. Bar-Cohen, p. 93-100 (5-8 March, 2001).

22. T. F. Otero and M. T. Cortes, "A sensing muscle," Sens Act B, 96 (1-2)**,** 152-156 (2003).

23. E. Smela, "Conjugated polymer actuators for biomedical applications," Adv. Mater., 15 (6)**,** 481-494 (2003).

24. E. Jager, W.H., O. Inganas, and I. Lundstrom, "Microrobots for Micrometer-Size Objects in Aqueous Media: Potential Tools for Single-Cell Manipulation," Science, 288, 2335-2338 (2000).

25. L. Bay, K. West, P. Sommer-Larsen, S. Skaarup, and M. Benslimane, "A conducting polymer artificial muscle with 12% linear strain," Adv. Mater., 15 (4), 310-313 (2003).

26. A. Della Santa, D. De Rossi, and A. Mazzoldi, "Characterization and modelling of a conducting polymer muscle-like linear actuator," Smart Mater. Struct., 6, 23 (1997).

27. X. Wang, B. Shapiro, and E. Smela, "Ion transport in conjugated polymers: Part 2. Model Development," J. Phys. Chem. B, submitted (2008).

28. X. Wang and E. Smela, "Ion transport in conjugated polymers: Part 1. Experimental studies on PPy(DBS)," J. Phys. Chem. B (submitted) (2008).

29. W. Wernet, M. Monkenbusch, and G. Wegner, "A new series of conducting polymers with layered structure: Polypyrrole n-alkylsulfates and n-alkylsulfonates," Makromol. Chem., Rapid Commun., 5, 157-165 (1984).

30. X. Wang, Shapiro, Benjamin, Smela, Elisabeth, "Visualizing Ion Currents in Conjugated Polymers," Advanced Materials, 16 (18), 1605-1609 (2004).

31. E. Smela and N. Gadegaard, "Volume change in polypyrrole studied by atomic force microscopy," J. Phys. Chem. B, 105, 9395-9405 (2001).

32. Y. Liu, Q. Gan, S. Baig, and E. Smela, "Improving PPy Adhesion by Surface Roughening," J. Phys. Chem. C, 111 (30), 11329-11338 (2007).

33. T. M. Swager, personal communication

34. E. Smela, H. Kariis, Z. Yang, M. Mecklenburg, and B. Liedberg, "Thiol Modified Pyrrole Monomers: 3. Electrochemistry of 1-(2-Thioethyl)-Pyrrole and 3-(2-Thioethyl)-Pyrrole Monolayers in Propylene Carbonate," Langmuir, 14 (11), 2984-2995 (1998).

35. E. Smela, "Thiol Modified Pyrrole Monomers: 4. Electrochemical Deposition of Polypyrrole over 1-(2-Thioethyl)-Pyrrole Monolayers," Langmuir, 14 (11), 2996-3002 (1998).

36. Y. Liu, Q. Gan, S. Baig, and E. Smela, "Preventing delamination of conjugated polymers due to electrochemical cycling," in preparation (2005).

37. E. Smela, "Microfabrication of PPy microactuators and other conjugated polymer devices," J Micromech Microeng, 9, 1-18 (1999).

38.   A. F. Diaz and K. K. Kanazawa, "Polypyrrole: An Electrochemical Approach to Conducting Polymers," in <u>Extended Linear Chain Compounds</u>, edited by J. S. Miller, p. 417-441 (Plenum Press, New York, 1983).

39.   M. Salmon, A. F. Diaz, A. J. Logan, M. Krounbi, and J. Bargon, "Chemical modification of conducting polypyrrole films," Molecular Crystals and Liquid Crystals, 83 (1)**,** 265-276 (1982).

40.   S. Skaarup, L. Bay, K. Vidanapathirana, S. Thybo, P. Tofte, and K. West, "Simultaneous anion and cation mobility in polypyrrole," Sol. State Ion., 159 (1-2)**,** 143-147 (2003).

41.   K. Naoi, Y. Oura, M. Maeda, and S. Nakamura, "Electrochemistry of surfactant-doped polypyrrole film(I) -- formation of columnar structure by electropolymerization," J. Electrochem. Soc., 142 (2)**,** 417 (1995).

42.   M. J. Ariza and T. F. Otero, "Ionic diffusion across oxidized polypyrrole membranes and during oxidation of the free-standing film," Colloids and Surfaces A**,** 226-231 (2005).

43.   J. T. Bendler, J. J. Fontanella, and M. F. Shlesinger, "Anomalous diffusion producing normal relaxation and transport," Journal of Physics: Condensed Matter, 19 (2007).

44.   Wikipedia, "Stretched exponential function", http://en.wikipedia.org/wiki/Stretched_exponential_function, 2008.

45.   S. Maw, E. Smela, K. Yoshida, and R. B. Stein, "Effects of monomer and electrolyte concentrations on actuation of PPy(DBS) bilayers," Synth. Met., 155 (1)**,** 18-26 (2005).

46.   X. Wang, B. Shapiro, and E. Smela, "Ion transport in conjugated polymers: Part 3. Model predictions," in preparation (2008).

47.   S. Shimoda and E. Smela, "The effect of pH on polymerization and volume change in PPy(DBS)," Electrochimica Acta, 44**,** 219-238 (1998).

48.   X. Wang, B. Shapiro, and E. Smela, "Ion transport in conjugated polymers: Part 4. Model predictions, oxidation of cation-transporting films," in preparation (2008).

49.   X. Wang and E. Smela, "Fast switching of conjugated polymer films," SPIE 13th Annual Int'l. Symposium on Smart Structures and Materials, EAPAD, San Diego, CA, (SPIE), vol. 6168, edited by Y. Bar-Cohen (Feb27 - Mar 2, 2006).

50.   Q. Pei and O. Inganäs, "Electrochemical applications of the bending beam method; a novel way to study ion transport in electroactive polymers," Sol. State Ion., 60**,** 161-166 (1993).

51.   E. Smela and N. Gadegaard, "Surprising volume change in PPy(DBS): an atomic force microscopy study," Adv. Mater., 11 (11)**,** 953-957 (1999).

52.   X. Wang and E. Smela, "Cycling conjugated polymers with different cations," SPIE 13th Annual Int'l. Symposium on Smart Structures and Materials, EAPAD, San Diego, CA, (SPIE), vol. 6168, edited by Y. Bar-Cohen (Feb27 - Mar 2, 2006).